AFRL-RX-WP-TP-2008-4353

MODELING OF MICROSTRUCTURE EVOLUTION DURING THE THERMOMECHANICAL PROCESSING OF TITANIUM ALLOYS (PREPRINT)

S.L. Semiatin and D.U. Furrer

Metals Branch
Metals, Ceramics, and NDE Division

JULY 2008

AIR FORCE RESEARCH LABORATORY
MATERIALS AND MANUFACTURING DIRECTORATE
WRIGHT-PATTERSON AIR FORCE BASE, OH 45433-7750
AIR FORCE MATERIEL COMMAND
UNITED STATES AIR FORCE

REPORT DOCUMENTATION PAGE

Form Approved
OMB No. 0704-0188

1. REPORT DATE *(DD-MM-YY)*	2. REPORT TYPE	3. DATES COVERED *(From - To)*
July 2008	Technical Paper Preprint	

4. TITLE AND SUBTITLE
MODELING OF MICROSTRUCTURE EVOLUTION DURING THE THERMOMECHANICAL PROCESSING OF TITANIUM ALLOYS (PREPRINT)

5a. CONTRACT NUMBER
In-house

5b. GRANT NUMBER

5c. PROGRAM ELEMENT NUMBER
62102F

6. AUTHOR(S)
S.L. Semiatin (AFRL/RXLMP)
D.U. Furrer (Rolls-Royce Corporation)

5d. PROJECT NUMBER
4347

5e. TASK NUMBER
RG

5f. WORK UNIT NUMBER
M02R2000

7. PERFORMING ORGANIZATION NAME(S) AND ADDRESS(ES)

Metals Branch (AFRL/RXLMP)
Metals, Ceramics, and NDE Division
Materials and Manufacturing Directorate
Wright-Patterson Air Force Base, OH 45433-7750
Air Force Materiel Command, United States Air Force

Rolls-Royce Corporation

8. PERFORMING ORGANIZATION REPORT NUMBER
AFRL-RX-WP-TP-2008-4353

9. SPONSORING/MONITORING AGENCY NAME(S) AND ADDRESS(ES)
Air Force Research Laboratory
Materials and Manufacturing Directorate
Wright-Patterson Air Force Base, OH 45433-7750
Air Force Materiel Command
United States Air Force

10. SPONSORING/MONITORING AGENCY ACRONYM(S)
AFRL/RXLMP

11. SPONSORING/MONITORING AGENCY REPORT NUMBER(S)
AFRL-RX-WP-TP-2008-4353

12. DISTRIBUTION/AVAILABILITY STATEMENT
Approved for public release; distribution unlimited.

13. SUPPLEMENTARY NOTES
Paper submitted to the ASM Handbook, Vol. 22–Modeling and Simulation: Processing of Metallic Materials. PAO Case Number: WPAFB 08-4313; Clearance Date: 14 Jul 2008. The U.S. Government is joint author of this work and has the right to use, modify, reproduce, release, perform, display, or disclose the work. Paper contains color.

14. ABSTRACT
Titanium and titanium alloys are widely used for a variety of aerospace, chemical, marine, and other specialty applications because of their high strength, low density, good ductility, fatigue and corrosion resistance, as well as other properties. Depending on the application, a specific property (or combination of properties) can be obtained through microstructural modification. Microstructure evolution and control in titanium alloys is heavily dependent on the allotropic transformation from a hexagonal-close-packed crystal structure (denoted as alpha phase) found at low temperatures to a body-centered-cubic crystal structure (denoted as beta phase) at high temperatures. For pure titanium, this occurs at 882 °C. In many titanium alloys, the beta phase is partially stabilized at lower temperatures, and the equilibrium volume fractions of alpha and beta vary with temperature. The temperature at which a specific alloy becomes entirely beta is called the beta transus. The conditions used for hot working and heating/heat treatment are often selected relative to the beta-transus temperature.

15. SUBJECT TERMS
titanium, alloy, modeling, microstructure, thermomechanical processing, crystal structure, beta transus

16. SECURITY CLASSIFICATION OF:			17. LIMITATION OF ABSTRACT:	18. NUMBER OF PAGES	19a. NAME OF RESPONSIBLE PERSON (Monitor)
a. REPORT	b. ABSTRACT	c. THIS PAGE			Sheldon L. Semiatin
Unclassified	Unclassified	Unclassified	SAR	78	19b. TELEPHONE NUMBER *(Include Area Code)* N/A

Standard Form 298 (Rev. 8-98)
Prescribed by ANSI Std. Z39-18

Modeling of Microstructure Evolution during the Thermomechanical Processing of Titanium Alloys

S.L. Semiatin* and D.U. Furrer*

Air Force Research Laboratory, AFRL/RXLM,
Wright-Patterson Air Force Base, OH 45433-7817
*Rolls-Royce Corporation, P.O. Box 420, Indianapolis, IN 46206-0420

INTRODUCTION

Titanium and titanium alloys are widely used for a variety of aerospace, chemical, marine, and other specialty applications because of their high strength, low density, good ductility, fatigue and corrosion resistance, as well as other properties. Depending on the application, a specific property (or combination of properties) can be obtained through microstructural modification.

Microstructure evolution and control in titanium alloys is heavily dependent on the allotropic transformation from a hexagonal-close-packed crystal structure (denoted as alpha phase) found at low temperatures to a body-centered-cubic crystal structure (denoted as beta phase) at high temperatures. For pure titanium, this occurs at 882°C. In many titanium alloys, the beta phase is partially stabilized at lower temperatures, and the equilibrium volume fractions of alpha and beta vary with temperature. The temperature at which a specific alloy becomes entirely beta (i.e., alpha + beta $\rightarrow$ beta) is called the beta transus. The conditions used for hot working and heating/heat treatment are often selected relative to the beta-transus temperature.

There are a number of important classes of titanium alloys, whose designations reflect the relative volume fraction of beta retained at room temperature. These include beta and near-beta alloys and near-alpha and

alpha/beta alloys [1, 2]. Beta and near-beta alloys have moderate to large amounts of beta-stabilizing elements such as vanadium, molybdenum, tungsten, niobium, chromium, and iron. The beta transi of near-beta alloys are typically in the range of 700 to 850°C [1]. Near-alpha and alpha/beta alloys have large amounts of alpha-stabilizing elements such as aluminum; the beta transi of near alpha and alpha/beta alloys are usually of the order of 950 to 1050°C [2].

The commercial processing of titanium alloys is most often based on an ingot-metallurgy approach in which large ingots are melted and refined using vacuum-arc or cold-hearth techniques, converted to mill products such as billet, plate, and sheet via a series of thermomechanical processing (TMP) steps, and fabricated into finished components via closed-die forging, superplastic forming, etc. [3, 4]. The TMP of ingots of alpha/beta and near-alpha titanium alloys comprises a large amount of hot work in the beta phase field, a small increment of hot work in the alpha+beta field, recrystallization heat treatment in the beta field, and secondary alpha+beta hot working [5]. The initial steps of the process (beta and initial alpha+beta working and beta recrystallization) are employed to transform the ingot structure of relatively large columnar beta grains into a structure of finer (~0.5 – 1 mm) recrystallized equiaxed beta grains. Secondary alpha+beta hot working and post hot-working alpha+beta annealing are then used to spheroidize the colony-alpha microstructure developed during cool-down of partially-converted billet products following the beta recrystallization heat treatment. The TMP of ingots and billets of near-beta titanium alloys usually

comprises hot working and recrystallization heat treatment in the beta phase field.

Irrespective of alloy class, the manufacture of finished components also typically includes a final heat treatment. These heat treatments are conducted in the alpha+beta or beta phase field and may be used to control the volume fraction and morphology of the equiaxed alpha phase (alpha/beta alloys), to develop a fully transformed, colony-alpha microstructure (alpha/beta alloys), or to control the volume fraction of acicular alpha (near-beta alloys) .

The modeling of microstructure evolution during the TMP of titanium alloys has seen significant advances during the last decade. Some of the principal efforts in this area have focused on the following:

- Recrystallization and grain growth phenomena for titanium alloys consisting of single-phase alpha or single-phase beta titanium.
- Dynamic and static spheroidization of colony alpha in alpha/beta titanium alloys during TMP in the alpha+beta phase field.
- Static and dynamic coarsening of equiaxed alpha or colony alpha in alpha/beta alloys during TMP in the alpha+beta phase field.
- The evolution of primary, equiaxed alpha and secondary (lamellar) alpha in alpha/beta titanium alloys during cooling following heat treatment in the alpha+beta phase field.
- The precipitation of acicular/lamellar alpha in alpha/beta and near-beta alloys following beta solution treatment.

The discussion below focuses on the modeling of microstructure evolution during TMP in the two-phase (alpha+beta) field for alpha/beta and beta titanium alloys. A companion article in this volume, “Modeling of Texture Evolution during the Thermomechanical Processing of Titanium Alloys” treats recrystallization and grain-growth phenomena in the single-phase alpha or beta fields inasmuch as such processes are strongly influenced by the dependence of nucleation and growth events on the local orientation of individual grains as well as the misorientation across grain boundaries. As such, microstructure and texture evolution are coupled and must be treated simultaneously during modeling. The evolution of deformation and transformation texture in alpha/beta titanium alloys during TMP in the alpha+beta field is also described in this latter article. The effect of microstructure and local texture on cavitation in alpha/beta titanium alloys during alpha+beta hot working is discussed in the article on “Modeling of Cavitation” in this volume.

DYNAMIC AND STATIC SPHEROIDIZATION

The breakdown of the colony-alpha microstructure during alpha+beta TMP plays a pivotal role in obtaining a uniform, fine equiaxed-alpha microstructure in forging bar stock and billet, plate for hog-out, and other alpha/beta titanium mill products (Figure 1). In the literature, the mechanism of this microstructure change has been ascribed to various recrystallization-like and spheroidization phenomena. Most of the research in this area has focused on the workhorse alloy of the aerospace titanium industry, Ti-6Al-4V.

A number of early observations [6, 7] suggested that recrystallized alpha grains are formed *within* the alpha lamellae during hot working or post-hot working annealing. Surface tension requirements do not permit 90° angles to exist between alpha/alpha boundaries (developed during recrystallization) and alpha-beta interfaces, however. Thus, a driving force is provided for the penetration of beta phase *along* the alpha/alpha boundaries and subsequent pinch-off/ segmentation of alpha lamellae.

The research of Weiss, *et al*. [8-10] expanded upon the work by Margolin and Cohen [6, 7], but did not invoke *recrystallized* alpha grains as the source of alpha-plate pinch-off. Rather, the main driving force was hypothesized to be the formation of intense shear bands within the alpha lamellae or the development of high-angle boundaries within alpha lamellae, spaced at periodic intervals along their length, due to dynamic/static recovery (Figure 2). If the strain is large enough, shear bands may lead to fracture and complete segmentation of an alpha lamella. In the absence of fracture, the alpha/alpha interfaces formed by shear bands or internal high-angle boundaries can give rise to surface-tension-driven penetration of the alpha plates by beta phase, as postulated by Margolin and Cohen. The rate of penetration by the beta phase depends on diffusion kinetics and the ratio of the interfacial energies of alpha/alpha boundaries and the alpha/beta interface.

Recent work by Salishchev, Furuhara, Stefansson, and their colleagues [12-15] has shed further light on some of the early observations. For example, Salishchev, *et al.* [12, 13] and Furuhara, *et al.* [14] used electron-backscatter-

diffraction (EBSD) imaging techniques to show that extended dynamic recovery during hot working (so-called *continuous* dynamic recrystallization) can give rise to sub-boundaries within the alpha plates. The misorientation across these boundaries increases with increasing hot deformation; at large strains, high-angle boundaries and a structure resembling recrystallized equiaxed-alpha grains are formed. High temperatures and low strain rates (~10^{-3} s^{-1}) favor such continuous-recrystallization behavior. Furthermore, it has been found that the size of the resulting alpha *particles* is of the same order of magnitude as the original platelet thickness, thus suggesting that beta phase may indeed penetrate along the high-angle boundaries developed in the alpha phase and result in complete segmentation of the original lamellae.

Stefansson and Semiatin [15] investigated static spheroidization behavior following hot working. During relatively short times, spheroidization of alpha platelets was found to be controlled by the pinch-off mechanism suggested by Margolin, Weiss, and their colleagues. At longer times, spheroidization was controlled by mass transport from the ends to the center of residual alpha platelets, thereby resulting in alpha particles whose diameter was substantially greater than the initial alpha platelet thickness.

Dynamic and static spheroidization observations for Ti-6Al-4V have provided the basis for mechanism-based models based on flow localization/shear banding/shear fracture, the pinch-off of alpha plates by beta, and spheroidization controlled by termination migration. Each of these is discussed below.

Flow Localization Analysis

Observations by Weiss, *et al.* [8] and Stefansson and Semiatin [11] have revealed that the spheroidization of colony alpha can occur by the localization of strain into intense shear bands within alpha lamellae (Figures 2b, c) that eventually leads to fracture and segmentation. The local shearing also produces relative local rotations of adjacent elements of a given alpha platelet, thereby providing a means of randomizing the orientation of equiaxed alpha particles and preventing microtexture, i.e., groups of alpha particles derived from a given prior colony of alpha plates each of which has a similar orientation.

The development of shear bands appears to be driven by the difficulty of accommodating deformation uniformly within hcp titanium due to its limited number of slip systems and the fact that the deformation resistance varies greatly among the possible slip systems. In particular, the critical resolved shear stress is relatively low for basal <a> and prism <a> systems, but considerably higher for the pyramidal <c+a> systems which must be activated to accommodate compression or extension along the c axis of hcp crystal structures at hot working temperatures [16]. Furthermore, the presence of beta phase between adjacent lamellae introduces a further anisotropy in slip behavior inasmuch as only one of the three <a> directions in the alpha phase is co-linear with a <111> slip direction in the beta phase [10]. Hence, one of alpha-phase <a> slip directions tends to be considerably softer than the other two at both hot- and cold-working temperatures [17, 18].

A simple analysis can be used to estimate the effect of non-uniformity in thickness along an alpha plate on the shear-localization rate. Although each alpha plate is surrounded by a layer of considerably softer beta, useful qualitative insight can be obtained by focusing solely on the deformation of alpha. The simplest case comprises simple shear along one slip system in a single alpha lamella. It is assumed that strain localization arises from regions in which the alpha plate is locally thinner than the rest. Denoting the thickness of the nominally uniform and thinner (defect) regions as t_u and t_d, respectively, equilibrium considerations [19] yield the following expression for a material whose constitutive behavior ($\tau = \tau(\Gamma, \dot{\Gamma})$, in which τ denotes shear stress as a function of shear strain Γ and shear strain rate $\dot{\Gamma}$) is characterized by a power-law strain-hardening and strain-rate hardening:

$$K \Gamma_u^n \dot{\Gamma}_u^m t_u = K \Gamma_d^n \dot{\Gamma}_d^m t_d \ , \qquad (1)$$

Here, K denotes the strength coefficient, n and m are the strain-hardening exponent and strain-rate sensitivity, and the subscripts u and d refer to the uniform and defect regions, respectively. Rewriting $\dot{\Gamma}$ as $d\Gamma/dt$, rearrangement of Equation (1) provides an expression relating the increments of shear strain in the uniform and defect regions, i.e., $d\Gamma_u$ and $d\Gamma_d$, respectively:

$$d\Gamma_d = d\Gamma_u (t_u \Gamma_u^n / t_d \Gamma_d^n)^{1/m} \ . \qquad (2)$$

Equation (2) can be solved numerically to relate Γ_u and Γ_d as a function of n and m and the magnitude of the thickness defect. Such solutions reveal that

large thickness non-uniformity (small values of t_d/t_u), low values of m, and low (or negative) values of n increase the kinetics of flow localization. An example calculation assuming typical values for the thickness inhomogeneity and material coefficients (i.e., a 10-pct. thickness defect ($t_d/t_u = 0.90$), m = 0.15, and n = 0) is shown in Figure 3. The results indicate a rapid, but not catastrophic, rate of flow localization; i.e., $d\Gamma_d/d\Gamma_u$ is relatively large but not infinite. This type of trend suggests that localization is likely terminated once Γ_d reaches a critical fracture strain.

Calculations such as that described above may be useful for interpreting dynamic spheroidization behavior at high strain rates (of the order of 0.1 s^{-1} or greater), in which flow softening (negative n) is enhanced by both microstructural influences [16] and deformation heating. In these cases, spheroidization kinetics have been found to depend very weakly on temperature *for a given perform microstructure* [20, 21]. This behavior may be rationalized qualitatively on the basis the compensatory effects of increases in both the thickness inhomogeneity (associated with decreasing average platelet thickness) *and* the strain-rate sensitivity with increasing temperature on localization kinetics. Further research documenting the kinetics of localization process, including the effect of local colony orientation and the orientation of neighboring colonies on spheroidization [22], is warranted. Detailed EBSD analysis of the activated slip systems that are associated with shear localization would also be beneficial. In this regard, it appears likely that systems whose slip planes form a large angle with each other

(e.g., prism and basal planes) must both undergo localization in order segment alpha lamellae into individual equiaxed particles.

Platelet Pinch-Off via Boundary Grooving

The penetration of beta phase along the boundaries formed within alpha platelets (or vice versa) can be analyzed using the classic approach for grain-boundary grooving developed originally by Mullins [23, 24]. In the original work, grooving was assumed to be controlled by volume diffusion, surface diffusion, or evaporation/condensation (as for a boundary meeting a free surface). The analysis is similar for all three cases. Thus, attention is focused here on the situation of most interest - the volume-diffusion-controlled grooving/penetration of alpha platelets by beta

Grooving is initiated by atomic-scale processes near the region of intersection of the alpha-alpha and alpha-beta boundaries. For the semi-infinite, two-dimensional case shown in Figure 4, these processes establish a groove angle δ which satisfies the equilibrium equation for the surface tensions associated with the two different interfaces [25], i.e.,

$$2\gamma_{\alpha\beta} \sin\delta = \gamma_{\alpha\alpha} \text{ ,} \qquad (3)$$

in which $\gamma_{\alpha\beta}$ and $\gamma_{\alpha\alpha}$ denote the surface energy of the alpha-beta interface and the alpha-alpha boundary within the alpha lamella. The development of the initial groove generates sharp edges of high energy adjacent to it. These asperities flatten rapidly leading to the diffusional development of a broad convex shape for the alpha-beta interface. The continued transport of mass from the curved alpha-beta interface to distant regions of lower curvature upsets the equilibrium

associated with the groove angle δ, and thereby drives the groove deeper. For a platelet of finite thickness, the mass transport continues until the groove has completely segmented the plate.

The Mullins grooving analysis [23, 24] determines the solute-concentration field that satisfies the steady-state diffusion (Laplace's) equation subject to appropriate boundary and initial conditions. For the case in which the platelet and matrix phases are both terminal solid solutions, the latter relations comprise the classical Gibbs-Thomson equation, the equilibrium equation (Equation (3) reformatted in terms of the groove slope), and the initial condition (an initially flat interface). Hence, the complete set of equations is as follows:

$$\nabla^2 C_\beta(x,y,t) = 0 \tag{4a}$$

$$\frac{C_\beta(R)}{C_\beta(R=\infty)} = 1 + \frac{\gamma_{\alpha\beta}\Omega}{k_B T R(x,t)} \tag{4b}$$

$$\frac{dW(0,t)}{dx} = m_g = \tan\delta \tag{4c}$$

$$W(x, t=0) = 0 \tag{4d}$$

In the above expressions, $C_\beta(R)$ and $C_\beta(R = \infty)$ denote the concentration of the rate-limiting solute in the matrix adjacent to a curved surface of radius R and a flat surface, respectively; Ω is the atomic volume, k_B is Boltzmann's constant, and T is the absolute temperature; W(x, t) is the interface shape as a function of the x coordinate and time t (Figure 4); and m_g is the slope of the groove at x=0.

The boundary-grooving analysis of Mullins reveals that the interface profile W(x, t) retains a fixed shape in normalized coordinates and that the groove

deepens as the cube root of time. The normalization constant is $(At)^{1/3}$, in which A is defined as:

$$A = \frac{C_\beta \gamma_{\alpha\beta} \Omega^2 D_\beta}{k_B T} = \frac{C_\beta \gamma_{\alpha\beta} V_M D_\beta}{R_g T} \quad . \qquad (5)$$

Here, D_β is the diffusivity of the solute through the matrix (beta) phase, V_M is the molar volume of the matrix, and R_g is the gas constant. The concentration C_β is defined in terms of atoms per unit volume or as an atomic fraction in the first and second expressions, respectively, for A. The time for the groove to move a distance d (relative to the plane y = 0, Figure 4) is then given by [24]:

$$d = 0.86\, m_g\, (At)^{1/3} \quad . \qquad (6)$$

For an alpha platelet of thickness d_α, the time to complete the boundary-grooving process is that corresponding to $d = d_\alpha/2$, inasmuch as beta-phase penetration would proceed inward from both alpha-beta interfaces. The time for pinch-off (t_p) is therefore

$$t_p = \frac{0.2 d_\alpha^3}{A\, m^3} \quad . \qquad (7)$$

Strictly speaking, the expressions for A (Equation (5)) and hence t_p (Equation (7)) are valid only when both the matrix phase and the second phase are terminal solid solutions. For Ti-6Al-4V, neither the alpha nor the beta phase is a terminal solid solution. In this case, two corrections are needed; one is required for the Gibbs-Thomson equation (Equation (4b)) and the other to account for the actual amount of solute which must be transported to deepen the groove. The two corrections are (1) $\{(1-C_\beta)\ /[(C_\alpha-C_\beta)(1 + \partial \ln r/\partial \ln C_\beta)]\}$, in which the second

parenthetical term in the denominator is a thermodynamic factor ($r \equiv$ activity coefficient of the solute in the beta phase) and (2) (C_α-C_β) [26]. In both terms, C_α denotes the concentration of the rate-limiting solute in the alpha phase. The term C_β in Equations (4b) and (5) is thus replaced by the *quotient* of these two terms [26], i.e.,

$$\text{Composition Factor, } C_F = \frac{C_\beta(1-C_\beta)}{(C_\alpha-C_\beta)^2[1+\partial \ln r/\partial \ln C_\beta]} \quad . \qquad (8)$$

Corrections such as that given in Equation (8) are particularly important for alloys such as Ti-6Al-4V in which there is only a small composition difference, $C_\beta - C_\alpha$.

The applicability of the Mullins analysis for the pinch-off of alpha platelets can be assessed using the static heat treatment observations of Stefansson and Semiatin [15]. In this work, it was found that boundary splitting was completed in ~14 h at 900°C and ~1 h at 955°C. At both temperatures, the slope m (tan δ) was measured as ~0.35. Input data at the lower and higher temperatures comprise the values of the composition factor (30.6, 61.3) [27], diffusivity of the rate-limiting solute (vanadium) (0.025, 0.05 $\mu m^2/s$) [28], and the alpha-platelet thicknesses (~1, 2 μm) [15]. The molar volume (10, 440 mm^3) and alpha-beta surface energy (0.4 J/m^2) are taken to be the same at both temperatures [27]. Applying Equation (7), the predicted time (1 h) is in excellent agreement with the observation for 955°C, but the prediction for 900°C (32 h) is approximately twice that observed. The difference between measured and predicted times for heat treatment at 900°C may be partially due to dislocation substructure in the beta matrix retained

from prior hot working and a concomitant enhancement in kinetics due to pipe diffusion.

Pipe diffusion may also play a role in the kinetics of the pinch-off of alpha platelets *during* deformation. In such cases, the required substructure within the alpha lamellae is developed at low-to-moderate strains, and grooving takes place at larger strains. If concurrent hot working enhances the diffusivity of solutes through the beta matrix by a factor of the order of 50, the times required for splitting alpha lamellae would be of the order of a minute at 955°C or 20 minutes at 900°C. Thus, the breakdown of the colony-alpha microstructure during deformation at low strain rates ($\leq 10^{-2}$ s^{-1}) may indeed involve an element of boundary grooving.

Static Spheroidization via Termination Migration

The complete breakdown of the colony-alpha microstructure via shear localization and/or boundary grooving usually requires strains much in excess of those that can be imposed in conventional production practices. Moreover, the dislocation substructure which drives boundary grooving during static heat treatment tends to be eliminated in relatively short times. At the completion of the pinch-off process, sections of alpha lamellae having a pancake-like shape remain. Subsequent (longer-time) completion of spheroidization occurs via termination migration; i.e., the transfer of solute from the periphery to the flat (plan) surfaces of each (assumed non-interacting) alpha lamella, resulting in equiaxed alpha particles whose diameters are substantially greater than the original platelet thickness [15].

The time to complete static spheroidization via termination migration can be estimated using an approach originally developed by Courtney and Malzahn Kampe [29] and later extended by Semiatin, *et al.* [30] for the specific geometry involved here. The analysis comprises a relatively simple application of the one-dimensional form of Fick's Law to solute diffusion at the beginning and intermediate points of the process:

$$\text{Flux, } J = - D_\beta \frac{dC_\beta}{dx} \ , \qquad (9)$$

in which C_β and D_β are taken to be the concentration and diffusivity of the rate-limiting solute.

As for the boundary-grooving analysis, solute concentration gradients are described with the aid of the Gibbs-Thompson relation, using the two principal radii of curvature of the alpha platelet. For example, in the beginning of the diffusional process, during which the plan surfaces of remnant lamellae are still relatively flat, the concentration *difference* between the edges and plan surfaces is the following:

$$[C_\beta (R=\infty)](\gamma_{\alpha\beta}\Omega/k_B T) \left(\frac{2}{d_\alpha} + \frac{1}{\frac{w}{2} + \frac{d_\alpha}{4}}\right) . \qquad (10)$$

Here, d_α and w are the platelet thickness and diameter, respectively, and the other symbols are as defined for Equation (4b). Geometrical considerations provide estimates of the diffusion distance (and hence concentration *gradient*) and the area through which the solute flux passes.

The final result for the spheroidization time, τ_{vd}, incorporating the composition-factor correction (Equation (8)) as above is the following:

$$\frac{\tau_{vd}}{\tau'} = \frac{\xi^3 - [0.328\xi^{7/3}\left(1+\sqrt{1-0.763\xi^{-4/3}}\right)^2]}{4[\frac{2(1+\xi)}{3(0.5-0.572\xi^{-1/3})} + \frac{0.5\xi^{1/3}+0.665\xi^{2/3}}{3(0.143+0.934\xi^{-1/3})}]} \qquad (11a)$$

in which

$$\xi \equiv (w/d_\alpha) + 0.5 \qquad (11b)$$

$$\tau' \equiv d_\alpha^3 R_g T/D_\beta C_F \gamma_{\alpha\beta} V_M \qquad (11c)$$

The dependence τ_{vd}/τ' on ξ of is shown in Figure 5a.

The validity of Equation (11) to quantify the spheroidization behavior and persistence of remnant lamellae was established by Semiatin, *et al.* [30] using observations for Ti-6Al-4V heat treated at 955°C (Figures 5b,c). At this temperature, the shapes of the lamellae that existed after the completion of boundary grooving (time ≈ 1h) approximated the idealized pancake geometry assumed in the diffusion model. For Ti-6Al-4V, the diffusion of vanadium through the beta matrix is rate-limiting in comparison to the diffusion of aluminum.

Model predictions of τ_{vd}/τ' and hence τ_{vd} for spheroidization of the remnant lamellae are given in Table I. The predicted values for the spheroidization time for the pancake-shape geometry ranged from approximately 5 to 15 hours for 5 of the 7 platelets; the other two lamellae were predicted to require times of the order of 30 hours. These values of spheroidization time compare well with the measured time of 12-14 hours to achieve approximately 90 volume pct. of spheroidized microstructure, as defined by alpha particles with an

aspect ratio of less than 2:1 [15, 30]. Thus, it is not surprising that a small volume fraction of modest aspect-ratio, partially-spheroidized lamellae would remain after 14 hours (Figure 5c).

Phenomenological Models

Because of the complexity of the various mechanisms that control the dynamic and static spheroidization of the colony-alpha microstructure, several attempts have been made to fit phenomenological models to measured data for the regime of processing parameters most common in production practice [31-34]. For example, the data of Stefansson, *et al.* [31] for the overall kinetics of static spheroidization following deformation at 900 or 955°C and a strain rate of 0.1 s^{-1} (Figure 6) have served as the basis for a phenomenological fit for the fraction spheroidized X_s as a function of temperature T and prestrain ε [32-34]:

$$X_s = (a\varepsilon + f) \log t + b\varepsilon + cT + d \text{ ,} \qquad (12)$$

in which a, b, c, d, and f are constants. Recent additional measurements by Brooks, *et al.* [34] have shown that static spheroidization kinetics are also dependent on the strain rate during the pre-deformation.

STATIC AND DYNAMIC COARSENING

The term coarsening refers to the increase in the average size of a dispersion of second-phase particles, lamellae, etc. during TMP. Also known as Ostwald ripening, coarsening in alpha/beta titanium alloys generally refers to the increase in the average size of equiaxed-alpha particles in the beta matrix or the increase in the average thickness of the lamellae within a colony-alpha microstructure. Such phenomena may occur during static preheating/heat

treatment or during deformation in the alpha+beta phase field. Several models have been developed and applied to quantify the static and dynamic coarsening of equiaxed alpha and the static coarsening of colony-alpha in alpha/beta titanium alloys.

Static Coarsening of Equiaxed Alpha

Static coarsening of a distribution of equiaxed particles in a matrix phase comprises the shrinkage (and elimination) of the smaller particles and the growth of the larger particles. The process is driven by the reduction of the total surface energy of the system. The rate of coarsening is frequently limited by diffusion of solutes through the matrix or by a reaction at matrix-particle interfaces.

Most approaches for describing coarsening are based on the classic work of Lifshitz, Slyosov, and Wagner (LSW) [26, 35, 36]. This early work assumed an infinitesimal volume fraction of particles and matrix/particle compositions which are both terminal solid solutions. For coarsening controlled by *bulk diffusion* of a solute through a matrix denoted as beta, the classical LSW theory predicts the following for the variation of the *average* radius of the particles ($\bar{r}_\alpha$) as a function of time t:

$$\bar{r}_\alpha^3 - \bar{r}_{\alpha o}^3 = \left[\frac{8 D_\beta \gamma_{\alpha\beta} C_\beta V_M}{9 R_g T}\right](t - t_o) = k_{LSW}\,(t - t_o) \qquad (13a)$$

in which D_β denotes the diffusivity in the beta matrix of the rate-limiting solute, $\gamma_{\alpha\beta}$ is the energy associated with particle-matrix (alpha-beta) interfaces (in J/m^2), C_β is the *equilibrium* concentration in the beta matrix of the rate-limiting solute (expressed as an atomic fraction), V_M is the molar volume of the particles, R_g is

the gas constant, T is the absolute temperature, and the subscript ‘o’ signifies quantities at an initial (reference) time. When coarsening is limited by a matrix-particle interface reaction, the coarsening exponent (exponent of $\bar{r}_\alpha$ in Equation (13a)) takes a value of 2 instead of 3. The bracketed term in Equation (13a) is known as the LSW rate constant k_{Lsw} :

$$k_{LSW} \equiv \frac{8 D_\beta \gamma_{\alpha\beta} C_\beta V_M}{9 R_g T} \quad . \tag{13b}$$

The form of the rate constant, k_{MLSW}, for a *finite* volume fraction of particles in a system comprising two concentrated alloy phases is the following [37, 38]:

$$k_{MLSW} = \frac{8 f(\phi) D_\beta \gamma_{\alpha\beta} C_\beta (1-C_\beta) V_M}{9 R T (C_\alpha - C_\beta)^2 [1 + \partial \ln r / \partial \ln C_\beta]} \quad , \tag{14}$$

in which $f(\phi)$ describes the functional dependence of the rate constant on volume fraction ϕ, C_α is the *equilibrium* concentration in the alpha particle of the rate-limiting solute (expressed as an atomic fraction), and r is the activity coefficient of the rate-limiting solute in the beta matrix. A number of analyses have been conducted to estimate $f(\phi)$ and hence the interaction of the solute sources/sinks comprising a field of second-phase particles and its effect on overall coarsening behavior [39]. As summarized by Doherty [38], the terms in Equation (14) which are related to the volume-fraction function $f(\phi)$ and the phase concentrations can readily increase the magnitude of predictions of the rate constant by one or two orders of magnitude.

The applicability of Equations (13) and (14) to describe the static coarsening of Ti-6Al-4V with an equiaxed-alpha microstructure was established by Semiatin, Sargent, and their coworkers for heat treatment temperatures between 775 and 955°C [27, 40]; typical microstructure observations are shown in Figure 7. The coarsening exponent was found to be 3 (Figure 8a), indicating that coarsening was indeed diffusion controlled. The ratio of the measured rate constant and the calculated value of $K_{MLSW}/f(\phi)$ for each temperature (and hence corresponding volume fraction) was determined to estimate $f(\phi)$. A comparison of the values of $f(\phi)$ so determined to various model predictions (Figure 8b) indicated that the Voorhees-and-Glicksman model [39] was most appropriate for quantifying the effect of volume fraction on coarsening kinetics for Ti-6Al-4V.

Dynamic Coarsening of Equiaxed Alpha

Coarsening of equiaxed alpha in alpha/beta titanium alloys may also occur *during* hot deformation (Figure 9). A number of investigations [40-42] have shown that the kinetics of coarsening in such situations are enhanced by approximately an order of magnitude relative to those for static coarsening. The effect is most noticeable at strain rates that characterize superplastic (or near-superplastic) flow, i.e., ~10^{-4} to 10^{-3} s^{-1}. Under these conditions, the time of deformation is typically of the order of 10 to 100 minutes.

As for static behavior, dynamic-coarsening kinetics have been found to be bulk-diffusion controlled with a coarsening exponent equal to 3 [42]. With respect to the coarsening constant, K_{MLSW}, an examination of Equation (14) suggests that

the principal factor that would be affected by concurrent deformation is the diffusivity D_β.

Defects such as dislocations and a non-equilibrium concentration of vacancies generated during deformation can contribute significantly to diffusion. Insight into the effect of such pipe diffusion on kinetics can be obtained from work on microalloyed steels [43]. For these materials, precipitation kinetics were found to increase by approximately two orders of magnitude during concurrent deformation at conventional strain rates (~0.1 – 1 s^{-1}); at these strain rates, the micro-mechanism of plastic flow is principally dislocation glide/climb. (Precipitation rates were found to increase by one order of magnitude during static heat treatment following a prestrain of 0.05.) By contrast, superplastic flow occurs in a regime in which deformation is accomplished largely by grain-boundary sliding and secondarily by dislocation-glide processes. Thus, the enhancement of diffusion during superplastic flow would be expected to be *less* than that during higher strain rate conventional forming. Thus, the observed increase in coarsening kinetics during superplastic flow by one, rather than two, orders of magnitude appears to be reasonable [40, 42].

Dynamic coarsening in alpha/beta titanium allows can have a significant effect on stress-strain behavior at superplastic strain rates [40-42]. Deformation occurs primarily by sliding at the alpha-beta interfaces, and the accommodation of resulting stress concentrations developed at triple points, grain edges, etc. becomes more difficult as the alpha particle size increases. Hence, dynamic

coarsening typically gives rise to flow hardening in stress-strain curves (Figure 10a).

An evolving microstructure should be taken into account when formulating constitutive models to describe plastic flow. One of the most widely-used constitutive approaches to relate flow stress σ and strain rate $\dot{\varepsilon}$ is the single state variable model of Bird, Mukherjee, and Dorn [44], typically applied for single-phase alloys:

$$\dot{\varepsilon} = \left(\frac{A_{BMD} D G_s b}{k_B T}\right)\left(\frac{\sigma}{G_s}\right)^{1/m}\left(\frac{b}{d}\right)^{p} \qquad (15)$$

In Equation (15), A_{BDM} is a constant, D is a diffusivity, k_B is Boltzmann's constant, T is absolute temperature, G_s is the shear modulus, b is the length of the Burgers vector, m is the rate sensitivity (1/m is the stress exponent of the strain rate), d is the grain size, and p is the grain size exponent of the strain rate. For superplastic flow characterized by gbs accommodated by glide/climb of dislocations, m ~ 0.5 and p ~ 2. For gbs accommodated by diffusional flow, m ~ 1 and p ~ 2 or 3, depending on whether bulk (lattice) or boundary diffusion predominates.

It has been shown that superplastic flow in two-phase alpha/beta titanium alloys can also be modeled using Equation (15), provided the *instantaneous* alpha particle size (accounting for dynamic coarsening) is used for 'd', and the values of G_s and b pertain to the softer beta phase [40]. In this respect, the alpha particles act like the core and the beta matrix like the mantle in the classical Gifkins model of superplastic flow [45]. To determine the appropriate diffusivity to be used in Equation (15), Sargent, *et al.* [40] inverted Equation (15) and plotted

log $A_{BMD}D$ as a function of 1/T using the measured values of stress, alpha particle size, m, and p corresponding to the imposed strain rates in the superplastic regime (Figure 10b). The resulting plot was linear, yielding an activation energy Q = 160 kJ/mol. This value of Q is comparable to that for the diffusion of vanadium (in annealed beta titanium), the solute which controls static (and dynamic) coarsening (Figure 10b). The comparison of the lines for $A_{BMD}D$ vs 1/T for superplastic flow and D_{β}^{V} suggests that A_{BMD} is of the order of 10 when D_{BMD} is taken to be equivalent to the diffusivity of vanadium in annealed beta titanium. By analogy with the relation between the rates of dynamic and static coarsening, A_{BDM} thus quantifies the enhancement of diffusion due to concurrent superplastic deformation.

Static Coarsening of Lamellar Alpha

The static coarsening/thickening of alpha lamellae in colony- or Widmansttten- (basketweave-) alpha microstructures represents an important consideration with regard to the control of the final alpha particle size in mill products of alpha/beta titanium alloys. This is because the sizes of alpha particles size are generally no smaller than the thickness of the alpha lamellae from which they originate. Furthermore, the ease of dynamic and/or static spheroidization is greatly dependent on the thickness of the lamellae, irrespective of whether the mechanism is boundary grooving or shear localization. Hence, an understanding of the kinetics of the coarsening of lamellar microstructures during static heat treatment is important.

Thickening of alpha lamellae during static heating occurs by mass transport which results in a reduction in overall surface area and thus surface energy. The transport may occur between a lamella and so-called “branches” which are attached to it as well as between adjacent lamellae due to a classical coarsening-type process (Figure 11). The former mechanism, i.e., branch elimination, is analogous to the phenomenon of “fault migration” treated previously in the literature [46, 47] and is relatively easy to quantify inasmuch as the entity which dissolves (a branch or lamellar fault) forms a well defined geometric relation with the lamella or lamellae onto which its mass is transferred (Figure 11a). By contrast, classical coarsening of an aggregate of lamellae (Figure 11b) is a much more difficult problem because of the irregular plan-view shapes of typical alpha platelets, the complex spatial arrangement of the platelets within a colony relative to each other, and the irregular shape of the colonies themselves [48]. Due to these complexities, a method to model the latter coarsening phenomenon has not yet been developed.

An approximate Fick’s Law treatment of the coarsening of colony alpha in alpha/beta titanium alloys via branch elimination has been performed recently [49]. The analysis is similar to that for static spheroidization via termination migration summarized earlier in this article. In brief, the concentration gradient and associated flux are determined using (1) the Gibbs-Thompson equation, assuming that the branch has a radius of curvature equal to one-half its thickness and the lamella onto which its mass is transferred is flat (Figure 11a), and (2) a composition factor (Equation (8)) to correct for the fact that the alpha and beta

phases are not terminal solid solutions. The branch recession rate is given by the following expression:

$$\frac{dL_b}{dt} = \frac{\pi D_\beta C_F V_M \gamma_{\alpha\beta}}{R_g T T_b (Y_b + T_b/2)} \qquad (16)$$

In this equation, the geometric factors are defined in Figure 11a; and D_β, C_F, V_M, $\gamma_{\alpha\beta}$, R_g, and T denote the diffusivity of the rate-limiting solute, the composition factor (Equation (8)), the molar volume of the alpha phase, the alpha-beta interface energy, the gas constant, and absolute temperature, respectively.

Predictions of the branch recession rate from Equation (16) show reasonably good agreement with observations after correcting for the stereological (section-plane) effect [49]. In particular, for a heat treatment at 955°C, the recession rate was predicted to be 7.5 mm/h for branches 1.66 μm thick lying 1.86 μm from the lamella to which they are attached. The measured recession rate was ~10 μm/h.

FINAL HEAT TREATMENT

Heat treatment is used to control final microstructure and properties and to relieve residual stresses for both alpha/beta and beta titanium alloys [50, 51]. For alpha/beta alloys, these treatments include (1) solution treatment at relatively high temperatures in the alpha+beta field followed by water quenching or air cooling, (2) so-called recrystallization treatment at slightly lower temperatures followed by slow cooling, (3) mill annealing at a temperature of the order of 700°C, and (4) beta annealing followed by water quenching, forced convection, etc. Each of these treatments may be followed with a final aging/stabilization heat

treatment. The principal final heat treatment for beta and near-beta alloys consists of aging of material previously beta annealed and water quenched.

In this section, two broad categories of heat-treatment models are discussed dealing with (1) microstructure evolution during cooling following alpha + beta solution treatment of alpha/beta titanium alloys with an equiaxed-alpha microstructure and (2) decomposition of beta following beta annealing of alpha/beta alloys or during the aging of beta titanium alloys.

Alpha+Beta Heat Treatment of Alpha/Beta Alloys

Final alpha+beta heat treatment of alpha/beta titanium alloys with an equiaxed-alpha microstructure is used to control the volume fraction and size of the primary alpha and the nature of the transformed matrix phase. To this end, components are typically solution treated high in the alpha+beta phase field and cooled via water quenching or forced convection. Because of section size variations, the cooling rate and hence microstructure vary within the component thereby leading to non-uniform properties. Predictive models can be very useful to quantify these variations.

Diffusion Analysis. A diffusion analysis can be applied to estimate the growth of primary alpha particles and the onset of the decomposition of residual beta during continuous cooling following alpha+beta solution treatment [52 - 54]. The approach is based on the “exact” one-dimensional solution for the growth of an isolated spherical precipitate as a function of time t and diffusivity D [55, 56] and consideration of the effect of soft impingement on the supersaturation controlling the rate of growth.

The diffusion solution is the following:

$$R(t) = 2\lambda(Dt)^{1/2} \text{ .} \qquad (17)$$

To treat continuous cooling, the differential form of Equation (17) is used, viz.:

$$dR/dt = 2\lambda^2 D/R \text{ .} \qquad (18)$$

In Equations (17) and (18), the parameter λ is given by the relation:

$$\{\lambda^2 \exp(\lambda^2)\} \bullet [\, (\exp(-\lambda^2)) - (\lambda\pi^{1/2}\mathrm{erfc}(\lambda))] = \Omega_s/2 \text{ ,} \qquad (19a)$$

in which Ω_s denotes the supersaturation:

$$\Omega_s = (C_M - C_I)/(C_P - C_I) \text{ .} \qquad (19b)$$

Here, C_M, C_I, and C_P represent the compositions of the matrix far from the matrix-particle interface, the matrix at the matrix-particle interface, and the particle at the matrix-particle interface, respectively. For a diffusion-controlled reaction, C_I and C_P correspond to the *equilibrium* matrix and particle compositions, respectively.

Equation (19a) is not readily inverted to obtain λ as a function of Ω_s. However, $\lambda = \lambda(\Omega_s)$ may be obtained from a simple FORTRAN program or using commercial software such as the 'Solver' tool of Microsoft Excel (Figure 12).

It should be mentioned that the approximate "constant-radius" diffusion solution [38, 57] yields a relation analogous to Equation (18), but with a pre-factor of Ω_s instead of $2\lambda^2$. Figure 12 shows that $2\lambda^2/\Omega_s$ is greater than unity even for relatively small values of the supersaturation Ω_s. Thus, the constant-radius solution underestimates the growth rate except for values of Ω approaching zero. Even for $\Omega_s < 0.1$ (the range of applicability often quoted in the literature),

substantial errors in the prediction of particle size are inevitable when using the constant-radius solution.

To simulate actual situations involving a collection of alpha particles, the interaction of the diffusion fields (i.e., the soft impingement effect) must be taken into account. In such cases, the 'far-field' matrix composition C_M is usually adjusted using an approximation derived from a mass balance [57]:

$$C_M = (C_o - f_\alpha C_\alpha)/(1 - f_\alpha) \text{ ,} \qquad (20)$$

in which C_o and f_α denote the overall alloy composition and the volume fraction of the precipitate/particle phase (i.e., primary alpha). Because the composition of the alpha phase in alloys such as Ti-6Al-4V often shows relatively little variation with temperature, the particle compositions C_α and C_P are equivalent and constant.

Numerical Solution. The solution of Equation (18) subject to the soft impingement criterion (Equation (20)) can readily be accomplished using a spreadsheet method. The required input data include the initial alpha particle radius, solution temperature/volume fraction of alpha phase, phase compositions, diffusivity as a function of temperature, and cooling rate [54]. The beta approach curve (showing the volume fraction of beta as a function of temperature) and phase compositions for Ti-6Al-4V are given in Figure 13. The diffusivity of aluminum and vanadium in beta titanium with a composition similar to that of beta in Ti-6Al-4V is as follows [28]:

$$\text{Aluminum: } D_\beta^{Al}(\mu m^2/s) = 199200 \exp(-18040/T(K)) \qquad (21a)$$

$$\text{Vanadium: } D_\beta^{V}(\mu m^2/s) = 77000 \exp(-17460/T(K)) \qquad (21b)$$

The instantaneous alpha particle radius R can be converted to volume fraction f_α using the following expression:

$$f_\alpha = f_{\alpha o}(R/R_o)^3 \qquad (22)$$

Here, $f_{\alpha o}$ and R_o denote the initial volume fraction and particle radius, respectively. The solution procedure then comprises the following steps:

(i) Specify initial temperature/volume fraction of alpha, initial alpha particle radius, diffusing element and its overall content (C_o), cooling rate, and time/temperature decrement

(ii) Impose a temperature/time decrement.

(iii) Calculate the supersaturation Ω_s (Equation (19b)) using measured equilibrium phase compositions for alpha and beta (e.g., Figure 13) and the matrix composition (C_M) determined from Equation (20).

(iv) Calculate λ (Equation (19a)) and the rate of change of the alpha-particle radius (Equation (18)).

(v) Impose a temperature/time decrement.

(vi) Calculate the new alpha particle radius and the volume fraction of alpha (Equation (22)).

(vii) Repeat steps (iii) – (vi) until the desired final temperature is reached.

The output of the spreadsheet calculations includes the alpha particle radius and supersaturation as a function of temperature.

The usefulness of the model for diffusional growth of equiaxed alpha following solution treatment high in the alpha + beta phase field has been verified

using Ti-6Al-4V [52]. Experiments and corresponding model calculations were conducted for several different peak temperatures (and hence initial volume fractions of alpha) and cooling rates. The model calculations were done assuming two different initial alpha particle radii which bounded those measured (4μm, 5 μm) and diffusion controlled by the supersaturation of aluminum or vanadium. Sample microstructural observations and model results for a peak (solution) temperature of 955°C and a cooling rate of 42°C/min are shown in Figure 14. Model predictions of the volume fraction of alpha as a function of temperature during cool-down tended to lie above the measurements. This behavior can be explained on the basis of the decomposition of the beta matrix during cooling, a factor which would reduce the supersaturation that drives the growth of primary alpha. A parameter known as the secondary alpha factor (which is a function of cooling rate, diffusivity and supersaturation) was derived therefore to predict the onset of beta transformation and the temperature below which diffusional growth of primary alpha would be retarded or cease [52].

Model Enhancements. A number of enhancements have been made to the diffusion model described above. These include the ability to treat the growth of primary alpha with (a) a pre-specified size distribution [53] or (b) a mixture of equiaxed and lamellar-platelet morphologies (such as would be present in material that is not fully spheroidized) [54]. The former work has shown that the *average* alpha particle size for an arbitrary initial size distribution varies with temperature in a manner identical to that predicted for an initial distribution of

mono-size particles, i.e., the case summarized above. The other effort revealed that lamellar alpha particles grow substantially slower than equiaxed particles.

The phase-field (PF) method has also been applied to obtain detailed information on the temporal *and* spatial evolution of alpha particle-size and shape during final alpha/beta heat treatment of titanium alloys with an equiaxed-alpha microstructure [58, 59]. The PF approach utilizes the numerical solution of (1) the generalized (Cahn-Hilliard) diffusion equation [60] in terms of chemical-potential gradients and chemical mobility (rather than concentration gradients and diffusivities) and (2) the time-dependent Ginzburg-Landau equation that describes structural changes that accompany phase transformations. Because of the use of chemical potentials in the analysis, an important factor in this approach is the estimation of the Gibbs free energy as a function of concentration, order parameter (i.e., phase), and their gradients; methods to calculate the Gibbs free energy for PF simulations are described in the article "Phase-Field Modeling for Solid-State Processes" in this volume. An example of the application of the PF method for the growth of primary alpha particles in a titanium alloy solution treated at 930°C and then rapidly cooled to and soaked at 900°C is shown in Figure 15. The results show noticeable differences in growth behavior for the cases of randomly- versus uniformly-spaced particles.

Beta Annealing and Beta Decomposition

The decomposition of single-phase beta serves as the basis for two types of common heat treatments: the beta annealing of alpha/beta titanium alloys and the aging of beta-annealed beta and near-beta alloys.

Alpha/Beta Titanium Alloys. The microstructure formed in alpha/beta titanium alloys which are beta-annealed is heavily dependent on the cooling rate. High rates give rise to a martensitic-type transformation, moderate rates to a basketweave/Widmanstatten microstructure, and slow rates to colony-alpha structure. The formation of the Widmanstatten and colony-alpha in alloys such as Ti-6Al-4V involves nucleation and growth of the alpha phase and has been modeled using both phenomenological and phase-field models.

Phenomenological models, which generally provide only temporal averages, have most often relied on the application of the Johnson-Mehl-Avrami-Kolmogorov (JMAK) approach [61, 62] and modifications of it. For example, a JMAK approach can be used to describe phase decomposition following beta annealing of alpha/beta alloys such as Ti-6Al-4V and Ti-6Al-2Sn-4Zr-2Mo-0.1Si (Ti6242Si) under both isothermal and continuous cooling conditions [63, 64]. In the simpler isothermal instance, the standard phenomenological JMAK relation is used to fit measurements:

$$X = 1 - \exp(-k\ t^{n_a}) \ , \tag{23}$$

in which X denotes the fraction transformed, the rate constant k is a function of temperature, t is time, and n_a denotes the JMAK (Avrami) exponent. Plots of log(ln[1/(1-X)]) versus log t are made to determine the Avrami exponent. In Reference 63, it was found that the values of n_a for both Ti-6Al-4V and Ti6242Si were between 1.15 and 1.6. The lower values (n_a ~ 1) pertained to isothermal transformation at temperatures from ~900 to 950°C, at which alpha nucleated heterogeneously at and grew from the beta grain boundaries; such values are in

agreement with classical predictions in the literature for continuous nucleation at grain-boundaries [65]. The higher n_a values were found for temperatures below 900°C at which alpha nucleated heterogeneously at the grain boundaries as well as homogeneously within the beta grains.

The interpretation of decomposition kinetics under *continuous-cooling* conditions can be somewhat more complex using the JMAK formalism. The challenge associated with such cases is best described by rewriting Equation (23) in terms of the explicit nucleation and growth rates, N and G, respectively:

$$X = 1 - \exp(-C_a N\ G^q t^{n_a}) \text{ ,} \qquad (24)$$

in which C_a and q are constants. The temperature dependence of N and G are both described by Arrhenius-type relations, i.e., N, G ~ $\exp(-Q/R_gT)$, in which Q is an activation energy, R_g is the gas constant, and T is absolute temperature. The activation energy for growth is relatively constant. However, Q for nucleation decreases with decreasing temperature [65], thus leading to a nucleation rate which rapidly increases with decreasing temperature and a complex function for the overall rate constant.

To simplify the modeling of beta decomposition under continuous-cooling conditions, therefore, an alternate approach based isothermal JMAK data can be applied [64]. Specifically, the fractions transformed under nominally isothermal conditions are summed for a series of closely-spaced temperature decrements. The calculation scheme makes use of a series of fictitious times each of which corresponds to that which would pertain if the entire fraction which had transformed at prior higher temperatures had occurred at the current

temperature. Using this basic approach, Malinov, *et al.* [64] developed a computer code to simulate continuous-cooling-transformation behavior of Ti-6Al-4V following beta annealing. It was assumed that n_a was constant (= 1.13); the code used an error-minimization routine to derive k = k(T) in the JMAK relation (Figure 16a). With this information, the computer simulation yielded predictions of transformed fractioned as a function of cooling rate and temperature in excellent agreement with measurements (Figure 16b).

Beta and Near-Beta Titanium Alloys. The precipitation of alpha from solution-treated beta and near-beta titanium alloys during isothermal or continuous-cooling heat treatments has been analyzed in detail by Da Costa Teixeira, Appolaire, and their coworkers [67-69]. In work similar to that of Malinov, *et al.* [63] for alpha/beta titanium alloys, a numerical method based on the incremental application of the JMAK relation was applied to quantify the cooling-transformation behavior of the beta-rich alloy Ti-17 [67]. The model treated the precipitation of grain-boundary alpha, Widmanstatten alpha that grew from the grain-boundary alpha, and Widmanstatten alpha which nucleated homogeneously with the beta grains.

More detailed mesoscale models which describe the temporal and some aspects of the spatial evolution of microstructure have also been developed for (1) isothermal transformation of an annealed equiaxed beta-grain microstructure [67] and (2) isothermal and cooling transformation of alloys with residual substructure from prior beta hot working [67].

The mesoscale model for isothermal transformation [68] focuses on four discrete phenomena: the nucleation of alpha at the beta grain boundaries (α_{gb}), the growth of this α_{gb}, the appearance of Widmanstatten-alpha sideplates (α_{wgb}) along the α_{gb}, and the growth of the α_{wgb}. Classical nucleation theory and Fick's Law are used to quantify the rate of nucleation and the planar growth of α_{gb}, respectively. The appearance of α_{wgb} sideplates is described empirically based on a critical thickness of the α_{gb}, and their growth is modeled using a diffusion approach analogous to that for α_{gb}.

Detailed transformation behavior is analyzed by implementing the various rate equations into a mesoscale simulation comprising 1,000 tetrakaidecahedral (14-faced) grains. To introduce a statistical aspect into the simulations, the beta grain-boundary energy (and hence the wetting angle of α_{gb}, nuclei) are varied from one grain boundary to another. Transition from one stage of the transformation to another at a specific grain boundary is based on several rules: (i) α_{gb} is allowed to grow once a grain boundary is covered 90 pct. by nuclei, and (ii) α_{wgb} sideplates are allowed to grow once the α_{gb} layer reaches the critical thickness. The growth of a given colony of α_{wgb} sideplates proceeds until the total transformed volume is equal to the size of the grain in which it is located or its length is equal to the grain size minus the length of any colony growing from an opposite grain boundary. Predictions of the fraction transformed as a function of time and the average number of colonies per beta grain show reasonably good agreement with measurements for the Beta-Cez alloy (Figure 17).

The mesoscale model and associated simulations for transformation of beta titanium alloys with residual substructure (subgrains) [69] are similar. The principal enhancements include: (i) modification of the geometric representation to include subgrain boundaries of various misorientations within the beta grains, (ii) nucleation of α_{gb} at both subgrain and grain boundaries at a rate dependent on boundary misorientation, and (iii) the appearance of α_{wgb} at a thickness of α_{gb} which depends on boundary misorientation. Simulation results revealed that it must be assumed that α_{wgb} plates are able to cross subgrain boundaries in order to approach the equilibrium volume fraction of alpha during long-time isothermal aging. With this assumption, good predictions of the dependence of transformation kinetics on subgrain size, number of colonies per grain, etc. are obtained for alloys such as Beta-Cez (Figure 18).

The phase-field technique has also been applied to investigate the decomposition of metastable beta to form colony- and basketweave- alpha microstructures [59, 70]. In this work, alpha sideplates were assumed to nucleate along grain-boundary-alpha layers (by the classic Mullins-Sekerka interface-instability mechanism [71]) and then grow into a supersaturated beta matrix. To this end, random fluctuations were introduced into the initial interface between the grain-boundary alpha and beta phase. Model results showed that the morphology of the alpha plates (breadth:thickness ratio) was sensitive to the assumed anisotropy in interfacial-energy and the elastic strain energy associated with semi-coherency of the alpha and beta phases. By introducing homogeneous nucleation (within beta grains), the evolution of microstructures containing both

alpha sideplatelets and Widmanstatten (basketweave) alpha within beta grains was simulated.

SUMMARY AND FUTURE OUTLOOK

Models to describe the evolution of microstructure during the thermomechanical processing of titanium alloys have been described. The mechanisms of spheroidization, coarsening, particle growth, and phase decomposition in titanium alloys frequently follow classical nucleation and diffusional-growth behaviors and thus are relatively easy to quantify. In this regard, accurate thermodynamic (phase equilibria) and kinetic data are key to the validation and application of the models for industrially-significant alloys. Avenues for future developments in this area are varied and include the following:

- Models for continuous dynamic recrystallization for both alpha titanium and beta titanium with applications to the dynamic spheroidization of lamellar-colony microstructures as well as for fully, wrought equiaxed microstructures.
- Internal-state variable models which describe concurrent plastic flow and the evolution of both micostructure and texture.
- Development of general models for thermodynamic, kinetic, and boundary properties needed for models of microstructure evolution.
- Coupled models of microstructure evolution and the formation/healing of defects such as cavities.

Acknowledgements- A large portion of this article was based on work conducted as part of the in-house research activities of the Metals Processing Group of the Air Force Research Laboratory's Materials and Manufacturing Directorate. The longstanding support and encouragement of the Laboratory management and the Air Force Office of Scientific Research (Drs. C.H. Ward, C.S. Hartley, B.P. Conner, and J. Fuller, program managers) are gratefully acknowledged. Technical discussions with many colleagues, including T.R. Bieler, R.D. Doherty, J.J. Jonas, N. Ma, F. Montheillet G.A. Salishchev, V. Seetharaman, N. Stefansson, Y. Wang, and I. Weiss, are also very much appreciated.

List of Symbols

a	slip vector along close-packed direction in hcp crystal structure
b	length of Burgers vector
C	composition (atomic fraction)
C_F	composition factor (Equation (8))
c	lattice parameter for hcp crystal structure
D	diffusivity
d_α	thickness of alpha platelet
d	grain/particle size
f_α	volume fraction of alpha
G	growth rate during phase transformation
G_s	shear modulus
J	mass flux
K	strength coefficient
k	rate constant in JMAK equation (Equation (23))
k_B	Boltzmann's constant
k_{LSW}	LSW coarsening rate constant
k_{MLSW}	LSW coarsening rate constant modified for volume-fraction effects
L_b	length of lamellar branch
N	nucleation rate during phase transformation
m	strain-rate sensitivity of the flow stress
m_g	slope of alpha-beta interface groove
n	strain-hardening exponent
n_a	JMAK (Avrami) exponent
p	grain size exponent of the strain rate
Q	activation energy
R	radius of curvature, particle radius
r_α	radius of globular alpha particle
r	activity coefficient
R_g	gas constant
T	absolute temperature
t	time
V_M	molar volume
W	boundary-groove interface shape, W = (x, t)
w	diameter of alpha platelet
X	fraction transformed
X_s	fraction spheroidized

x,y,z	cartesian coordinates
α	alpha phase
β	beta phase
Γ	shear strain
$\dot{\Gamma}$	shear strain rate
γ	surface energy (grain boundary, interface phase, etc.)
δ	groove angle
ε, $\dot{\varepsilon}$	normal/principal strain, strain rate
ϕ	volume fraction
λ	particle-growth parameter (Equations (17) and (18))
σ	normal/principal stress
Ω	atomic volume
Ω_s	supersaturation (Equation (19b))
τ	shear stress
τ_{VD}	time for diffusional spheroidization via termination migration

REFERENCES

1. I. Weiss and S.L. Semiatin, "Thermomechanical Processing of Beta Titanium Alloys - An Overview," *Materials Science and Engineering*, 1998, vol. A243, pp. 46.
2. I. Weiss and S.L. Semiatin, "Thermomechanical Processing of Alpha Titanium Alloys - An Overview," *Materials Science and Engineering*, 1999, vol. A263, p. 243.
3. Choudhury and E. Weingartner, "Vacuum Arc Remelting", in *ASM Handbook, Volume 15: Casting*, ASM International, Materials Park, OH, 1988, pp 406-408.
4. G. Luetjering and J.C. Williams, *Titanium*: Springer Verlag, Berlin, 2007.
5. S.L. Semiatin, V. Seetharaman, and I. Weiss, “Hot Working of Titanium Alloys- An Overview,” *Advances in the Science and Technology of Titanium Alloy Processing*, I. Weiss, *et al.*, eds., TMS, Warrendale, PA, 1997, pp. 3-73.

6. H. Margolin and P. Cohen, "Evolution of the Equiaxed Morphology of Phases in Ti-6Al-4V", *Titanium '80: Science and Technology*, H. Kimura and O. Izumi, eds., TMS, Warrendale, PA, 1980, pp. 1555-1561.
7. H. Margolin and P. Cohen, "Kinetics of Recrystallization of Alpha in Ti-6Al-4V", *Titanium '80: Science and Technology*, H. Kimura and O. Izumi, eds., TMS, Warrendale, PA, 1980, pp.2991-2997.
8. I. Weiss, G.E. Welsch, F.H. Froes, and D. Eylon, "Mechanisms of Microstructure Refinement in Ti-6Al-4V", *Titanium: Science and Technology*, G. Luetjering, U. Zwicker, and W. Bunk, eds., Deutsche Gesellschaft fur Metallkunde e.V., Oberursel, Germany, 1985, pp. 1503-1510.
9. I. Weiss, F.H. Froes, D. Eylon, and G.E. Welsch, "Modification of Alpha Morphology in Ti-6Al-4V by Thermomechanical Processing", *Metall. Trans. A*, 1986, vol. 17A, pp. 1935-1947.
10. G. Welsch, I. Weiss, D. Eylon, and F.H. Froes, "Lamellar to Equiaxed Grain Structure by Torsional Deformation of Ti-6Al-2Sn-4Zr-2Mo Alloy," *Advances in the Science and Technology of Titanium Alloy Processing*, I. Weiss, *et al.*, eds., TMS, Warrendale, PA, 1997, pp. 169-183.
11. N. Stefansson and S.L. Semiatin, Unpublished Research, Air Force Research Laboratory, Wrigth-Patterson Air Force Base, OH, 2001.
12. G.A. Salishchev, S.V. Zherebtsov, S. Yu. Mironov, and S.L. Semiatin, "Formation of Grain Boundary Misorientation Spectrum in Alpha-Beta Titanium Alloys with Lamellar Structure Under Warm and Hot Working," *Materials Science Forum*, 2004, vols. 467-470, pp. 501-506.

13. S. Zherebtsov, M. Murzinova, S. Mironov, G. Salishchev, and S.L. Semiatin, "Microstructure Refinement in Ti-6Al-4V during Warm Deformation," *Collected Proceedings, 2008 TMS Annual Meeting, Volume I: Materials Processing and Properties*, TMS, Warrendale, PA, 2008, pp. 211-217 (pdf only).
14. T. Furuhara, B. Poorganji, H. Abe, and T. Maki, "Dynamic Recovery and Recrystallization in Titanium Alloys by Hot Deformation," *JOM*, January 2007, vol. 59(1), pp. 64- 67.
15. N. Stefansson and S.L. Semiatin, "Mechanisms of Globularization of Ti-6Al-4V during Static Heat Treatment," *Metall. Mater. Trans. A*, 2003, vol. 34A, pp. 691-698.
16. S.L. Semiatin and T.R. Bieler, "Effect of Texture and Slip Mode on the Anisotropy of Plastic Flow and Flow Softening During Hot Working of Ti-6Al-4V ," *Metall. Mater. Trans. A*, 2001, vol. 32A, pp. 1787-1799.
17. A.A. Salem and S.L. Semiatin, "Hot Deformation of Ti-6Al-4V Single-Colony Samples," submitted to *Inter. J. Plasticity*, 2008.
18. S. Suri, G.B. Viswanathan, T. Neeraj, D.-H. Hou, and M.J. Mills, "Room Temperature Deformation and Mechanisms of Slip Transmission in Oriented Single-Colony Crystals of an Alpha/Beta Titanium Alloy," *Acta Mater.*, 1999, vol. 47, pp. 1019-1034.
19. S.L. Semiatin and J.J. Jonas, *Formability and Workability of Metals: Plastic Instability and Flow Localization*, ASM International, Materials Park, OH, 1984.

20. S.L. Semiatin, V. Seetharaman, and I. Weiss, "Flow Behavior and Globularization Kinetics During Hot Working of Ti-6Al-4V With a Colony Alpha Microstructure," *Materials Science and Engineering*, 1999, vol. A263, pp. 257-271.

21. E.B. Shell and S.L. Semiatin, "Effect of Initial Microstructure on Plastic Flow and Dynamic Globularization During Hot Working of Ti-6Al-4V," *Metall. Mater. Trans. A*, 1999, vol. 30A, pp. 3219-3229.

22. T.R. Bieler and S.L. Semiatin, "The Origins of Heterogeneous Deformation During Hot Working of Ti-6Al-4V," *Inter. J. Plasticity*, 2002, vol. 18, pp. 1165-1189.

23. W.W. Mullins, “Theory of Thermal Grooving,” *J. Applied Physics*, 1957, vol. 28, pp. 333-339.

24. W.W. Mullins, “Grain-Boundary Grooving by Volume Diffusion,” *Trans. TMS-AIME*, 1960, vol. 218, pp. 354-361.

25. G.L.J. Bailey and H.C. Watkins, “Surface Tensions in the System Solid-Copper-Molten Lead,” *Proc. Phys. Society*, 1950, vol. B63, pp. 350-358.

26. J.W. Martin, R.D. Doherty, and B. Cantor: *Stability of Microstructure in Metallic Systems*, Cambridge University Press, Cambridge, UK, 1997.

27. S.L. Semiatin, B.C. Kirby, and G.A. Salishchev, “Coarsening Behavior of an Alpha-Beta Titanium Alloy,” *Metall. Mater. Trans. A*, 2004, vol. 35A, pp. 2809-2819.

28. S.L. Semiatin, T.M. Brown, T.A. Goff, P.N. Fagin, D.R. Barker, R.E. Turner, J.M. Murry, J.D. Miller, and F. Zhang, “Diffusion Coefficients for Modeling the

Heat Treatment of Ti-6Al-4V," *Metall. Mater. Trans. A*, 2004, vol. 35A, pp. 3015-3018.

29. T.H. Courtney and J.C. Malzahn Kampe, "Shape Instabilities of Plate-Like Structures - II. Analysis," *Acta Metall.*, 1989, vol. 37, pp. 1747-1758.
30. S.L. Semiatin, N. Stefansson, and R.D. Doherty, "Prediction of the Kinetics of Static Globularization of Ti-6Al-4V," *Metall. Mater. Trans. A*, 2005, vol. 36A, pp. 1372-1376.
31. N. Stefansson, S.L. Semiatin, and D. Eylon, "The Kinetics of Static Globularization of Ti-6Al-4V," *Metall. Mater. Trans. A*, 2002, vol. 33A, pp. 3527-3534.
32. A.F. Wilson, V. Venkatesh, R. Pather, J.W. Brooks, and S.P. Fox, "The Prediction of Microstructure Development during Ti-6Al-4V Billet Manufacture," *Ti-2003: Science and Technology*, G. Luetjering and J. Albrecht, eds., Wiley-VCH Verlag GmbH, 2004, pp. 321-329.
33. J.W. Brooks, M.D. Griffiths, A.J. Storton, and R. Waddingham, "Modeling Microstructure Development – Measurement and Validation," *Proceedings, Materials Science and Technology 2006 (MS&T'06)*, TMS, Warrendale, PA, 2006, pp. pp. 595-606.
34. J.W. Brooks, M. Mulyadi, and M. Rist, "Constitutive Based Modeling of the Alpha Lath Width and Spheroidization in Ti-6-4," TMS Annual Meeting, New Orleans, LA, March 2008.

35. I.M. Lifshitz and V.V. Slyozov, “The Kinetics of Precipitation from Supersaturated Solid Solutions,” *J. Phys. Chem. Solids*, 1961, vol. 19, pp. 35-50.

36. C. Wagner, “Theory of Precipitate Change by Redissolution,” *Zeit. Elektrochem.*, 1961, vol. 65, pp. 581-591.

37. H. A. Calderon, P.W. Voorhees, J.L. Murray, and G. Kostorz, “Ostwald Ripening in Concentrated Alloys,” Acta M*etall. et Mater.*, 1994, vol. 42, pp. 991-1000.

38. R.D. Doherty, “Diffusive Phase Transformations in the Solid State,” *Physical Metallurgy*, R.W. Cahn and P. Haasen, eds., North-Holland, Amsterdam, 1996, ch. 15.

39. P.W. Voorhees and M.E. Glicksman, “Solution to the Multi-Particle Diffusion Problem with Applications to Ostwald Ripening – II. Computer Simulations,” *Acta Metall.*, 1984, vol. 32, pp. 2001-2011.

40. G.A. Sargent, A.P. Zane, P.N. Fagin, A.K. Ghosh, and S.L. Semiatin, “Low-Temperature Coarsening and Plastic-Flow Behavior of an Alpha/Beta Titanium Billet Material with an Ultrafine Microstructure,” submitted to *Metall. Mater. Trans. A*, 2008.

41. A.K. Ghosh and C.H. Hamilton, “Mechanical Behavior and Hardening Characteristics of a Superplastic Ti-6Al-4V Alloy,” *Metall. Trans. A*, 1979, vol. 10A, pp 699-706.

42. S.L. Semiatin, M.W. Corbett, P.N. Fagin, G.A. Salishchev, A.K. Ghosh, And C.S. Lee, “Dynamic-Coarsening Behavior of an Alpha-Beta Titanium Alloy,” *Metall. Mater. Trans. A*, 2006, vol. 37A, pp. 1125-1136.

43. I. Weiss and J.J. Jonas, “Interaction between Recrystallization and precipitation during the High Temperature Deformation of HSLA Steels,” *Metall. Trans. A*, 1979, vol. 10A, pp. 831-840.

44. J.E. Bird, A.K. Mukherjee, and J. E. Dorn, “Correlations between High-Temperature Creep Behavior and Structure,” *Quantitative Relation Between Microstructure and Properties*, D.G. Brandon and A. Rosen, eds., Israel Universities Press, Jerusalem, Israel, 1969, pp. 255-342.

45. R.C. Gifkins, “Grain-Boundary Sliding and Its Accommodation during Creep and Superplasticity,” *Metall. Trans. A*, 1976, vol. 7A, pp. 1225-1232.

46. L.D. Graham and R.W. Kraft, “Coarsening of Eutectic Microstructures at Elevated Temperatures,” *Trans. TMS-AIME*, 1966, vol. 236, pp. 94-102.

47. H.E. Cline, “Shape Instabilities of Eutectic Composites at Elevated Temperatures,” *Acta Metall.*, 1971, vol. 19, pp. 481-490.

48. N. Vanderesse, E. Maire, M. Darrieulat, F. Montheillet, M. Moreaud, and D. Jeulin, “Three-Dimensional Microtomographic Study of Widmanstatten Microstructures in an Alpha/Beta Titanium Alloy,” *Scripta Mater.*, 2008, vol. 58, pp. 512-515.

49. S.L. Semiatin and P.S. Poteet, “Branch Elimination during Heat Treatment of Titanium Alloys with a Colony-Alpha Microstructure,” submitted to *Metall. Mater. Trans. A*, 2008.

50. J.C. Williams and E.A. Starke, Jr., "The Role of Thermomechanical Processing in Tailoring the Properties of Aluminum and Titanium Alloys", *Deformation, Processing, and Structure*, G. Krauss, ed., ASM International, Materials Park, OH, 1984, pp. 279-354.
51. G.W. Kuhlman, "A Critical Appraisal of Thermomechanical Processing of Structural Titanium Alloys", *Microstructure/Property Relationships in Titanium Aluminides and Alloys*, Y-W. Kim and R.R. Boyer, eds., TMS, Warrendale, PA, 1991, pp. 465-491.
52. S.L. Semiatin, S.L. Knisley, P.N. Fagin, F. Zhang, and D.R. Barker, "Microstructure Evolution during Alpha-Beta Heat Treatment of Ti-6Al-4V," *Metall. Mater. Trans. A*, 2003, vol. 34A, pp. 2377-2386.
53. J.D. Miller and S.L. Semiatin, "Effect of the Size Distribution of Alpha Particles on Microstructure Evolution during Heat Treatment of an Alpha/Beta Titanium Alloy," *Metall. Mater. Trans. A*, 2005, vol. 36A, pp. 259-262.
54. S.L. Semiatin, T.M. Lehner, J.D. Miller, R.D. Doherty, and D.U. Furrer, "Alpha/Beta Heat Treatment of a Titanium Alloy with a Non-Uniform Microstructure," *Metall. Mater. Trans. A*, 2007, vol. 38A, pp. 910-921.
55. H.S. Carslaw and J.C. Jaeger, *Conduction of Heat in Solids*, Oxford University Press, London, 1959.
56. H.B. Aaron, D. Fainstein, and G.R. Kotler, "Diffusion-Limited Phase Transformations: A Comparison and Critical Evaluation of the Mathematical Approximations," *J. Appl. Physics*, 1970, vol. 41, pp. 4404-4410.

57. O. Grong and H.R. Shercliff, “Microstructural Modeling in Metals Processing,” *Progress in Materials Science*, 2002, vol. 47, pp. 163-282.

58. Q. Chen, N. Ma, K. Wu, and Y. Wang, “Quantitative Phase Field Modeling of Diffusion-Controlled Precipitate Growth and Dissolution in Ti-6Al-4V,” *Scripta Mater.*, 2004, vol. 50, pp. 471-476.

59. Y. Wang, N. Ma, Q. Chen, F. Zhang, S.-L. Chen, and Y.A. Chang, “Predicting Phase Equilibrium, Phase Transformation, and Microstructure Evolution in Titanium Alloys,” *JOM*, September 2005, vol. 57(9), pp. 32-39.

60. J.W. Cahn and J.E. Hilliard, “Free Energy of a Nonuniform System: I. Interfacial Energy,” *J. Chemical Physics*, 1958, vol. 28, pp. 258-267.

61. M. Avrami: “Kinetics of Phase Change: I. General Theory,” *J. Chemical Physics*, 1939, vol. 7, pp. 1103-1112.

62. W.A. Johnson and R.F. Mehl: “Reaction Kinetics in Processes of Nucleation and Growth,” *Trans. AIME*, 1939, vol. 135, pp. 416-430.

63. S. Malinov, P. Markovsky, W. Sha, and Z. Guo, “Resistivity Study and Computer Modeling of the Isothermal Transformation Kinetics of Ti-6Al-4V and Ti-6Al-2Sn-4Zr-2Mo-0.08Si Alloys,” *J. Alloys and Compounds*, 2001, vol. 314, pp. 181-192.

64. S. Malinov, Z. Guo, W. Sha, and A. Wilson: “Differential Scanning Calorimetry Study and Computer Modeling of Beta-to-Alpha Transformation in a Ti-6Al-4V Alloy,” *Metall. Mater. Trans. A*, 2001, vol. 32A, pp. 879-887.

65. J.W. Cahn, “The Kinetics of Grain Boundary Nucleated Reactions,” *Acta Metall.,* 1956, vol. 4, pp. 449-59.

66. J.W. Christian, *The Theory of Transformation in Metals and Alloys: Equilibrium and General Kinetic Theory*, 2nd edition, Pergamon Press, Oxford, UK, 1975.

67. J. Da Costa Teixeira, B Appolaire, E. Aeby-Gautier, S. Denis, G. Cailletaud, and N. Spath, "Transformation Kinetics and Microstructures of Ti17 Titanium Alloy during Continuous Cooling," *Materials Science and Engineering A*, 2007, vol. A448, pp. 135-145.

68. B. Appolaire, L. Hericher, and E. Aeby-Gautier, "Modeling of Phase Transformation Kinetics in Ti Alloys – Isothermal Treatments," *Acta Mater.*, 2005, vol. 53, pp. 3001-3011.

69. J. Da Costa Teixeira, B Appolaire, E. Aeby-Gautier, S. Denis, and F. Bruneseaux, "Modeling of the Effect of the Beta-Phase Deformation on the Alpha-Phase Precipitation in Near-Beta Titanium Alloys," *Acta Mater.*, 2006, vol. 54, pp. 4261-4271.

70. N. Ma, F. Yang, C. Shen, G. Wang, G.B. Viswanathan, P.C. Collins, D. Xu, R. Yang, H.L. Fraser, and Y. Wang, "Modeling Formation of Alpha Sideplates in Alpha/Beta Ti Alloys – Effect of Interfacial Energy Anisotropy and Coherency Elastic Strain Energy," *Titanium 2007: Science and Technology*, M. Ninomi, S. Akiyama, M. Ikeda, M. Hagiwara, K. Maruyama, eds., Japan Institute of Metals, Tokyo, 2007, pp. 287-290.

71. W.W. Mullins and R.F. Sekerka, "Morphological Stability of a Particle Growing by Diffusion or Heat Flow," *J. Applied Physics*, 1963, vol. 34, pp. 323-329.

Table I. Geometry of Remnant Alpha Lamellae and Model Predictions of Globularization Time at 955°C [30]

Lamella ID	Lamella Diameter, w (μm)	Lamella Thickness, t (μm)	η	τ_{vd}/τ'	τ_{vd} (h)
A	16.4	2.7	6.5	1.39	6.1
B	17.7	3.2	6.1	1.13	7.8
C	18.2	3.6	5.5	0.84	8.6
D	21.8	3.6	6.5	1.39	14.4
E	24.1	2.3	11.1	6.16	15.6
F	27.3	3.6	8.0	2.52	26.1
G	33.2	2.3	15.1	13.6	34.4

Figure Captions

Figure 1. Microstructures developed in Ti-6Al-4V during primary processing: (a) optical and (inset) SEM BSE micrographs of the colony-alpha microstructure and (b) SEM BSE micrograph of the fine, equiaxed-alpha microstructure. In SEM micrographs taken via backscattered-electron (BSE) imaging, the dark phase is alpha, and the lighter phase is beta (or very fine transformed beta).

Figure 2. Mechanisms of the spherodization of alpha lamellae: (a) spheroidization driven by the formation of sub-boundaries or shear bands within alpha lamellae [9] and (b, c) observation of shear bands developed during hot deformation [8, 11].

Figure 3. Predictions of a flow localization calculation for shear banding/shear fracture. The arrows indicate the strain in the nominally uniform region at which a hypothetical fracture strain is reached in the defect region.

Figure 4. Schematic illustration of the geometry during boundary grooving [23, 24].

Figure 5. Static spheroidization via termination migration: (a) Plot of τ_{vd}/τ' as a function of ξ and (b, c) SEM backscattered micrographs of the microstructure developed in Ti-6Al-4V samples deformed at 955°C to an effective strain of 1.1 and water quenched after holding at temperature for (a) 1 h or (b) 14 h [30]. The letters adjacent to the

unspheroidized alpha platelets in (b) correspond to the data in Table I. (Alpha ~ darker phase, beta ~ lighter phase).

Figure 6. Statically-spheroidized fraction of colony-alpha microstructure as a function of time during heat treatment at 955°C following pre-deformation to various strains at 955°C [31].

Figure 7. SEM backscattered micrographs taken at the same magnification illustrating static coarsening of Ti-6Al-4V (with an equiaxed-alpha microstructure) which was heat treated at 900°C and water quenched after times of (a) 1, (b) 4, (c) 16, (d) 48, or (e) 144 hours [27]. (Alpha ~ darker phase, beta ~ lighter phase)

Figure 8. Static-coarsening behavior of Ti-6Al-4V with an equiaxed-alpha microstructure [27]: (a) Coarsening kinetics in terms of average alpha particle size as a function of time and (b) comparison of the ratio of the measured coarsening rate at different temperatures (and hence volume fractions ϕ) and the calculated value of $K_{MLSW}/f(\phi)$ to various model predictions [39] to determine $f(\phi)$.

Figure 9. SEM backscattered micrographs taken at the same magnification illustrating dynamic coarsening of Ti-6Al-4V samples with an equiaxed-alpha microstructure deformed at 900°C, 10^{-4} s^{-1} to true strains of (a) 0, (b) 0.5, and (c) 1.4, followed by water quenching [42]. The compression axis is vertical for each micrograph. (Alpha ~ darker phase, beta ~ lighter phase)

Figure 10. Effect of dynamic coarsening on plastic flow of Ti-6Al-4V with an equiaxed-alpha microstructure [40]: (a) Selected flow curves and (b) constitutive analysis to determine the appropriate activation energy and diffusivity to describe superplastic flow.

Figure 11. Static coarsening of a colony-alpha microstructure in Ti-6Al-4V: (a) SEM backscattered micrograph illustrating lamellar branching observed at 955°C and the idealized geometry used to describe the microstructure [49] and (b) SEM backscattered micrographs of samples heat treated at 955°C for times of 0.25 or 48 h followed by water quenching.

Figure 12. Dependence of the growth parameter λ^2 and the ratio $2\lambda^2/\Omega_s$ on the supersaturation Ω_s [52].

Figure 13. Phase equilibria data for Ti-6Al-4V with a regular interstitial level: (a) Beta-approach curve and (b) phase compositions [52].

Figure 14. Alpha/beta heat treatment results for Ti-6Al-4V: (a,b,c) SEM backscattered micrographs of samples solution treated at 955°C, cooled at 42°C/min, and water quenched at the temperatures (T_q) indicated and (d) comparison of corresponding measurements of the volume fraction of primary alpha (data points) and diffusion-model predictions (lines) [52].

Figure 15. Phase-field model predictions of the growth of primary alpha in a titanium alloy which was solution treated at 930°C then cooled rapidly

and soaked isothermally at 900°C. Simulations were done for an initial alpha-particle distribution that was random or uniform [59].

Figure 16. Application of the JMAK relation to predict cooling-transformation behavior of Ti-6Al-4V following beta annealing: (a) Fitted dependence of the rate constant k on temperature and (b) comparison of predicted and measured transformed fractions as a function of cooling rate and temperature [64].

Figure 17. Comparison of measured (solid lines, data points) and predicted (broken lines) isothermal transformation kinetics for the titanium alloy Beta-Cez [68].

Figure 18. Comparison of measurements (data points, gray lines) and mesocale-model predictions (black lines) of microstructure evolution in Beta-Cez: (a) Isothermal transformation kinetics at 800°C for material prior beta worked to develop different subgrain sizes and (b) number of colonies observed in a 2D section as a function of time at 790°C for material pre-deformed 25 pct. in the beta phase field at a strain rate of 0.01 s^{-1} [69].

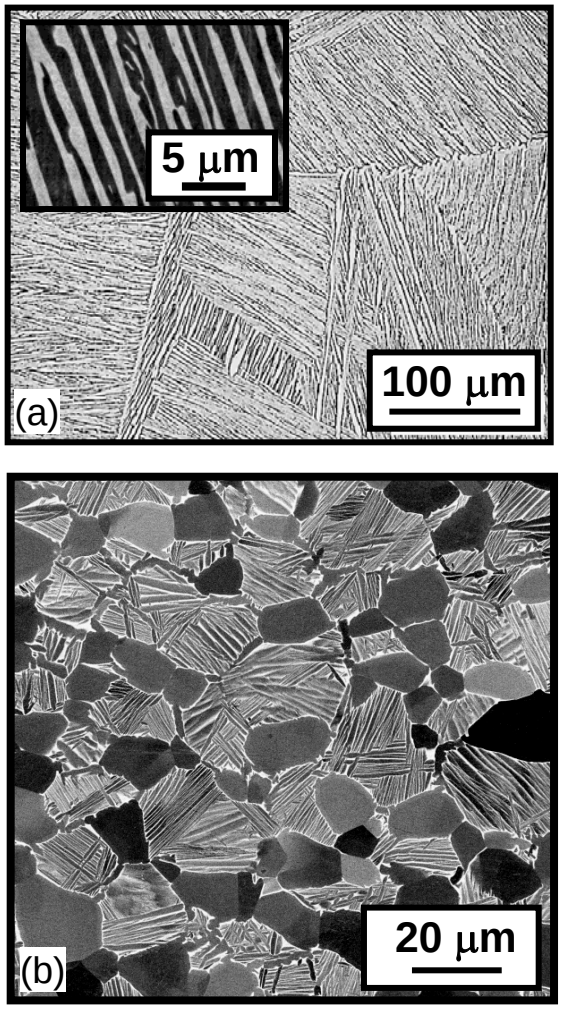

Figure 1. Microstructures developed in Ti-6Al-4V during primary processing: (a) optical and (inset) SEM BSE micrographs of the colony-alpha microstructure and (b) SEM BSE micrograph of the fine, equiaxed-alpha microstructure. In SEM micrographs taken via backscattered-electron (BSE) imaging, the dark phase is alpha, and the lighter phase is beta (or very fine transformed beta).

(a)

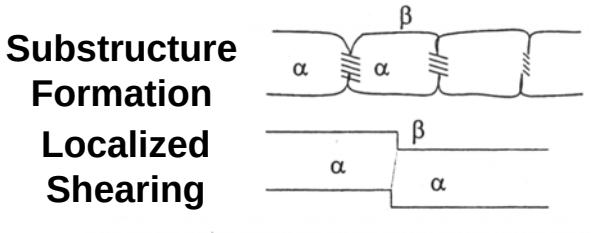

(b)

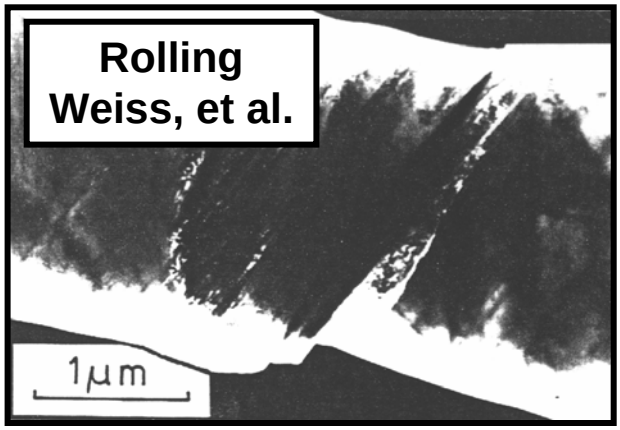

(c)

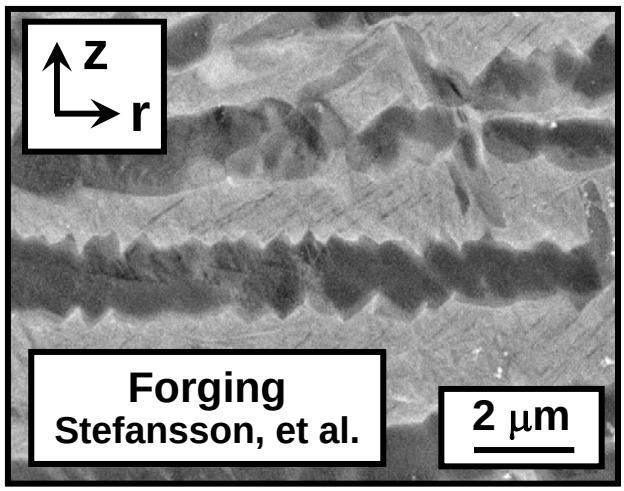

Figure 2. Mechanisms of the spherodization of alpha lamellae: (a) spheroidization driven by the formation of sub-boundaries or shear bands within alpha lamellae [9] and (b, c) observation of shear bands developed during hot deformation [8, 11].

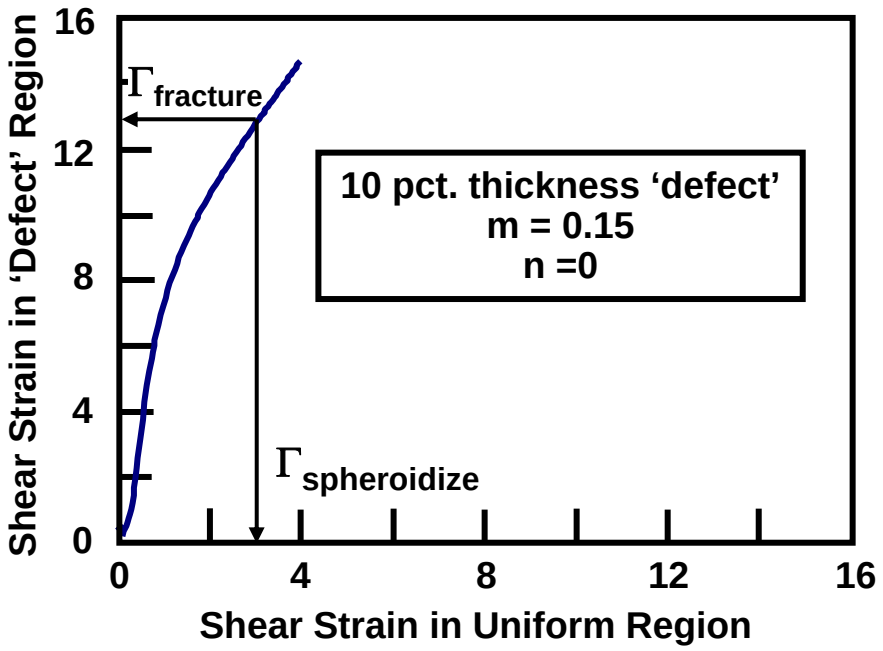

Figure 3. Predictions of a flow localization calculation for shear banding/shear fracture. The arrows indicate the strain in the nominally uniform region at which a hypothetical fracture strain is reached in the defect region.

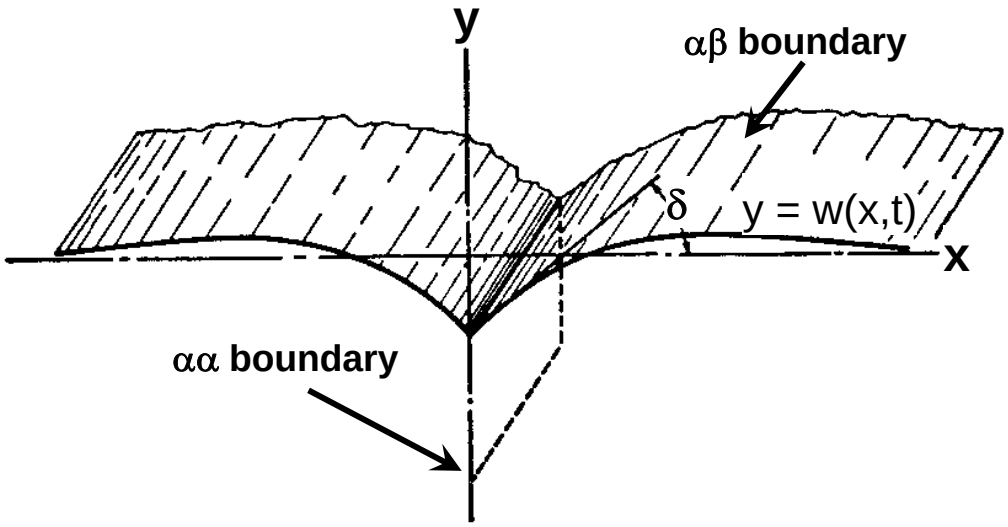

Figure 4. Schematic illustration of the geometry during boundary grooving [23, 24].

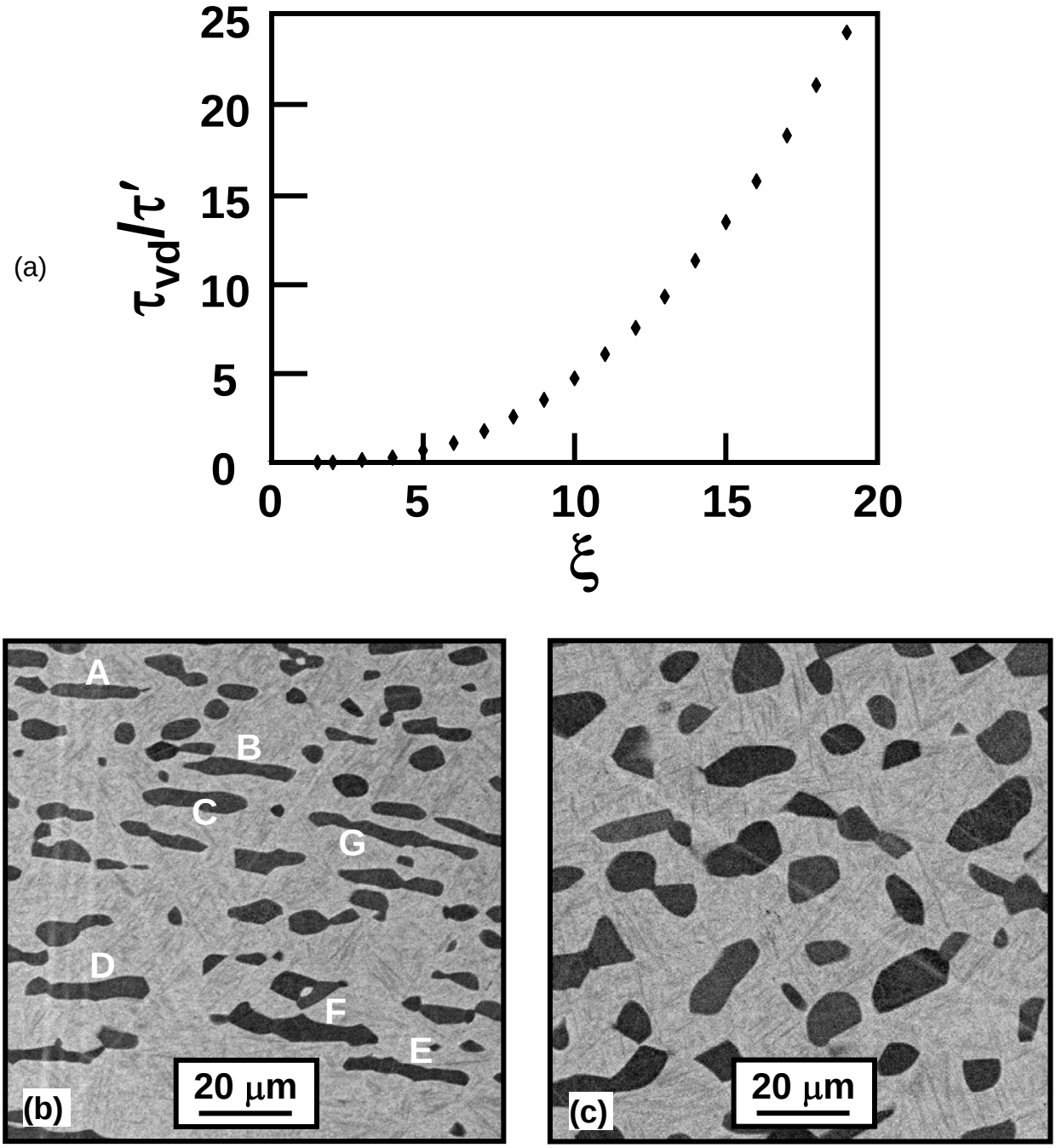

Figure 5. Static spheroidization via termination migration: (a) Plot of τ_{vd}/τ' as a function of ξ and (b, c) SEM backscattered micrographs of the microstructure developed in Ti-6Al-4V samples deformed at 955°C to an effective strain of 1.1 and water quenched after holding at temperature for (a) 1 h or (b) 14 h [30]. The letters adjacent to the unspheroidized alpha platelets in (b) correspond to the data in Table I. (Alpha ~ darker phase, beta ~ lighter phase).

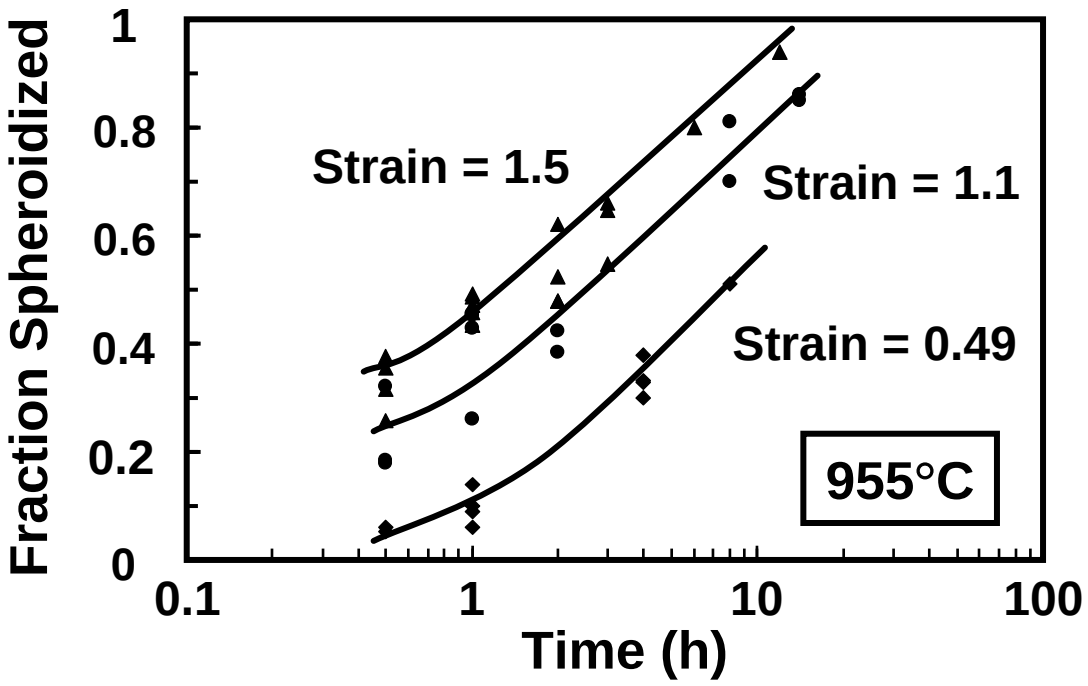

Figure 6. Statically-spheroidized fraction of colony-alpha microstructure as a function of time during heat treatment at 955°C following pre-deformation to various strains at 955°C [31].

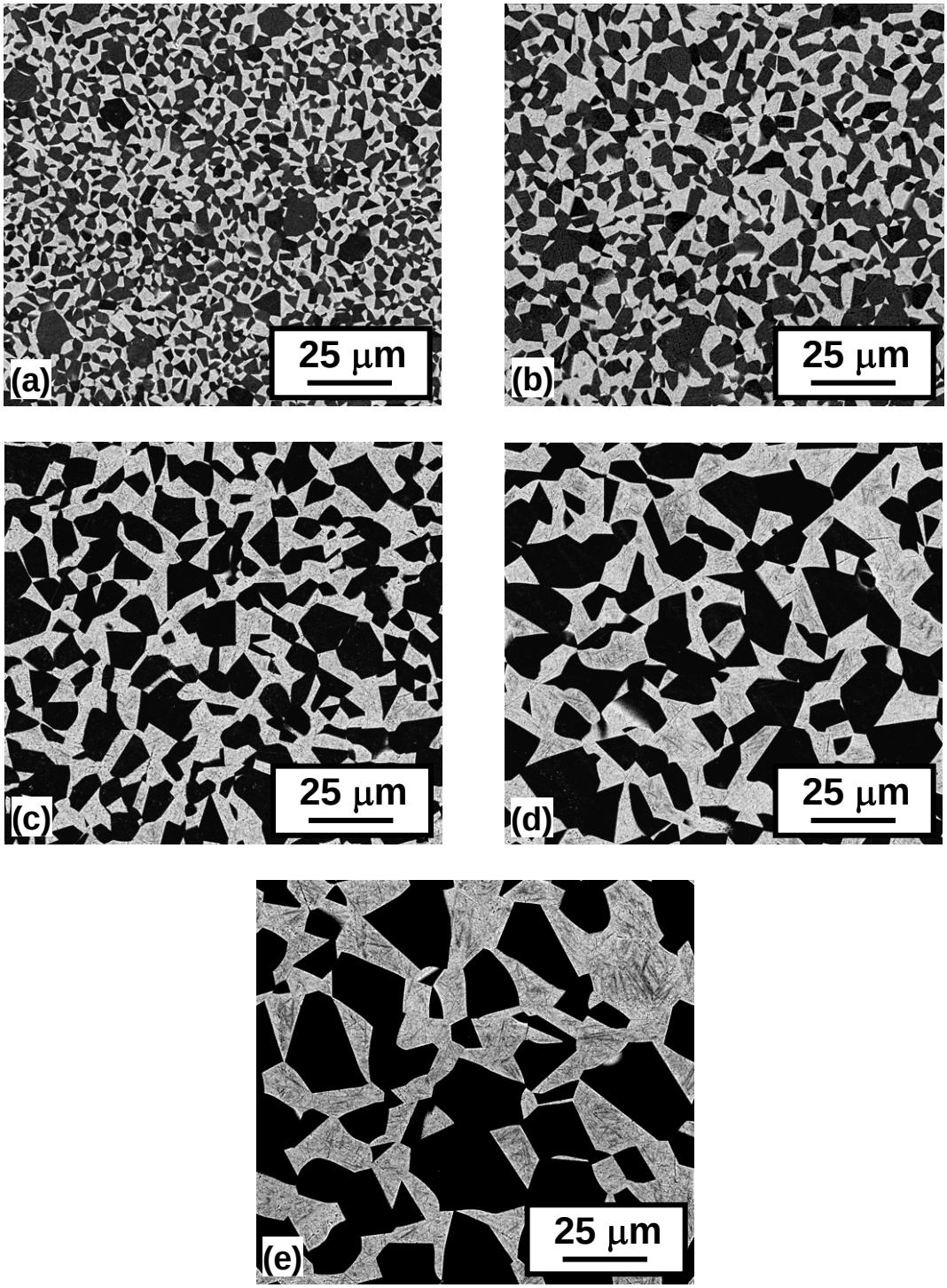

Figure 7. SEM backscattered micrographs taken at the same magnification illustrating static coarsening of Ti-6Al-4V (with an equiaxed-alpha microstructure) which was heat treated at 900°C and water quenched after times of (a) 1, (b) 4, (c) 16, (d) 48, or (e) 144 hours [27]. (Alpha ~ darker phase, beta ~ lighter phase)

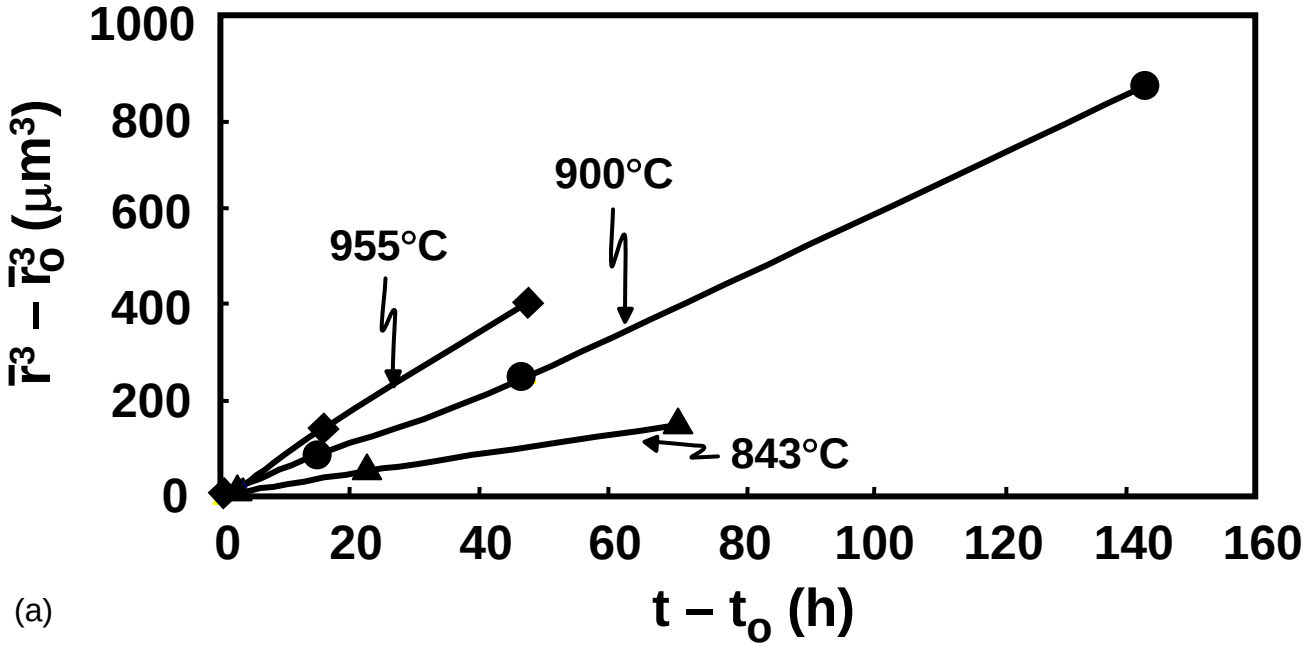

(a)

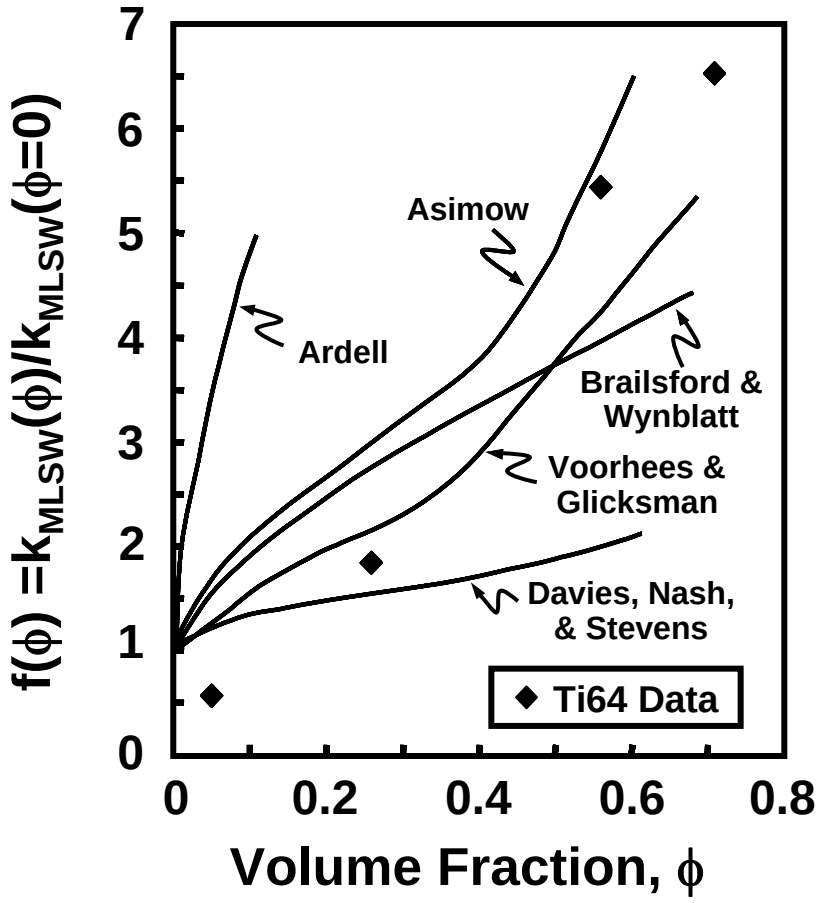

(b)

Figure 8. Static-coarsening behavior of Ti-6Al-4V with an equiaxed-alpha microstructure [27]: (a) Coarsening kinetics in terms of average alpha particle size as a function of time and (b) comparison of the ratio of the measured coarsening rate at different temperatures (and hence volume fractions ϕ) and the calculated value of $K_{MLSW}/f(\phi)$ to various model predictions [39] to determine $f(\phi)$.

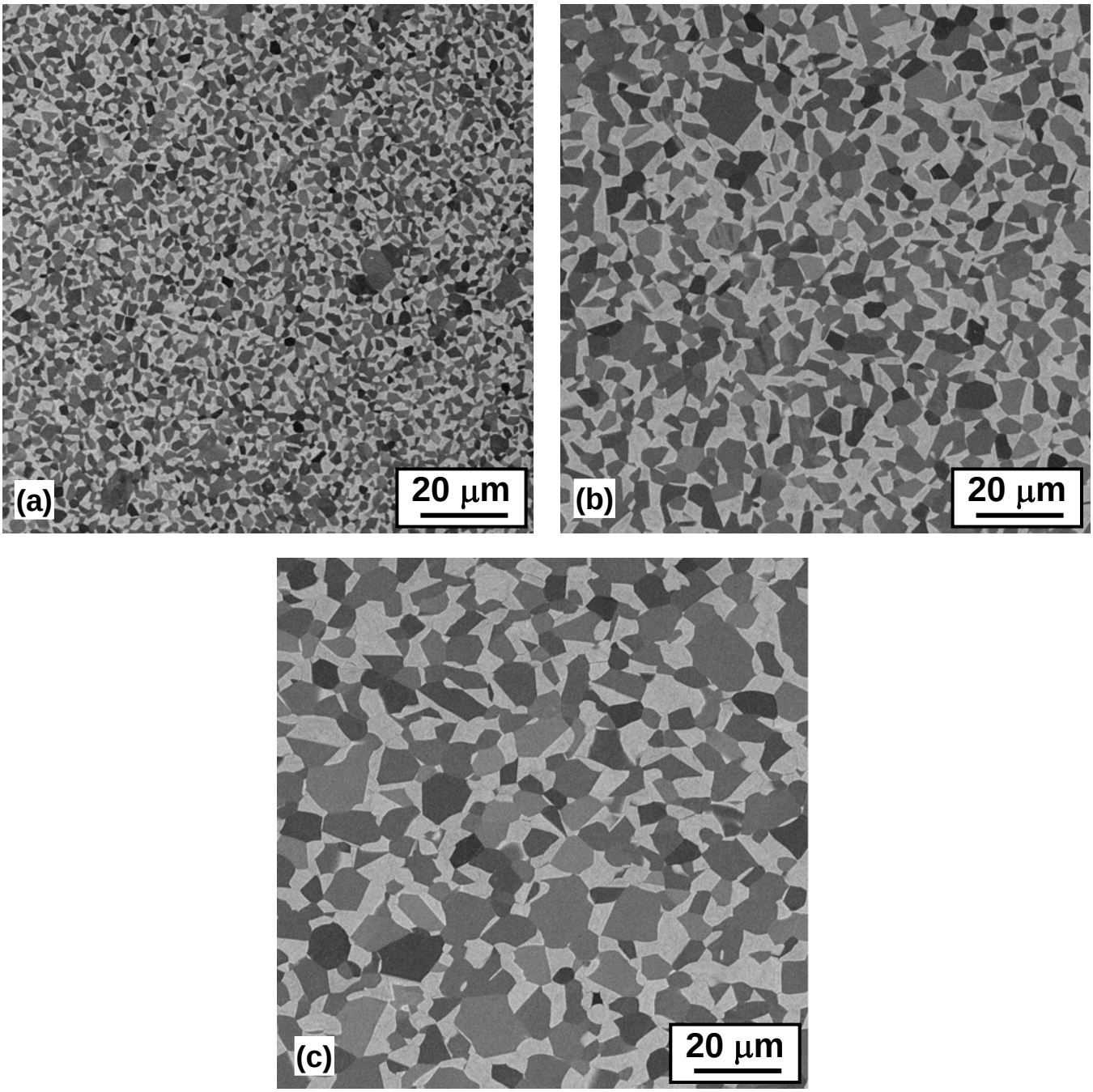

Figure 9. SEM backscattered micrographs taken at the same magnification illustrating dynamic coarsening of Ti-6Al-4V samples with an equiaxed-alpha microstructure deformed at 900°C, 10^{-4} s^{-1} to true strains of (a) 0, (b) 0.5, and (c) 1.4, followed by water quenching [42]. The compression axis is vertical for each micrograph. (Alpha ~ darker phase, beta ~ lighter phase)

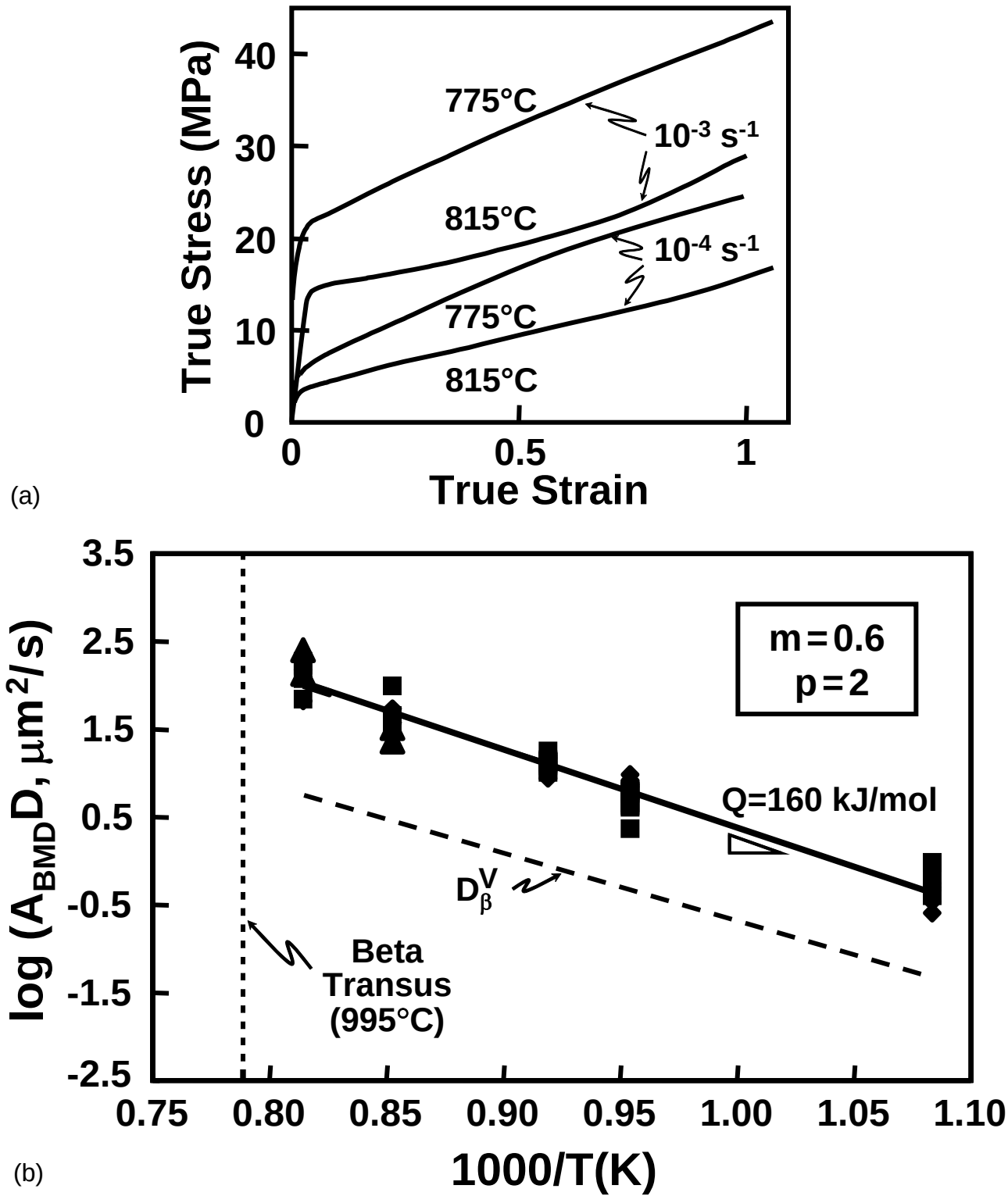

Figure 10. Effect of dynamic coarsening on plastic flow of Ti-6Al-4V with an equiaxed-alpha microstructure [40]: (a) selected flow curves and (b) constitutive analysis to determine the appropriate activation energy and diffusivity to describe superplastic flow.

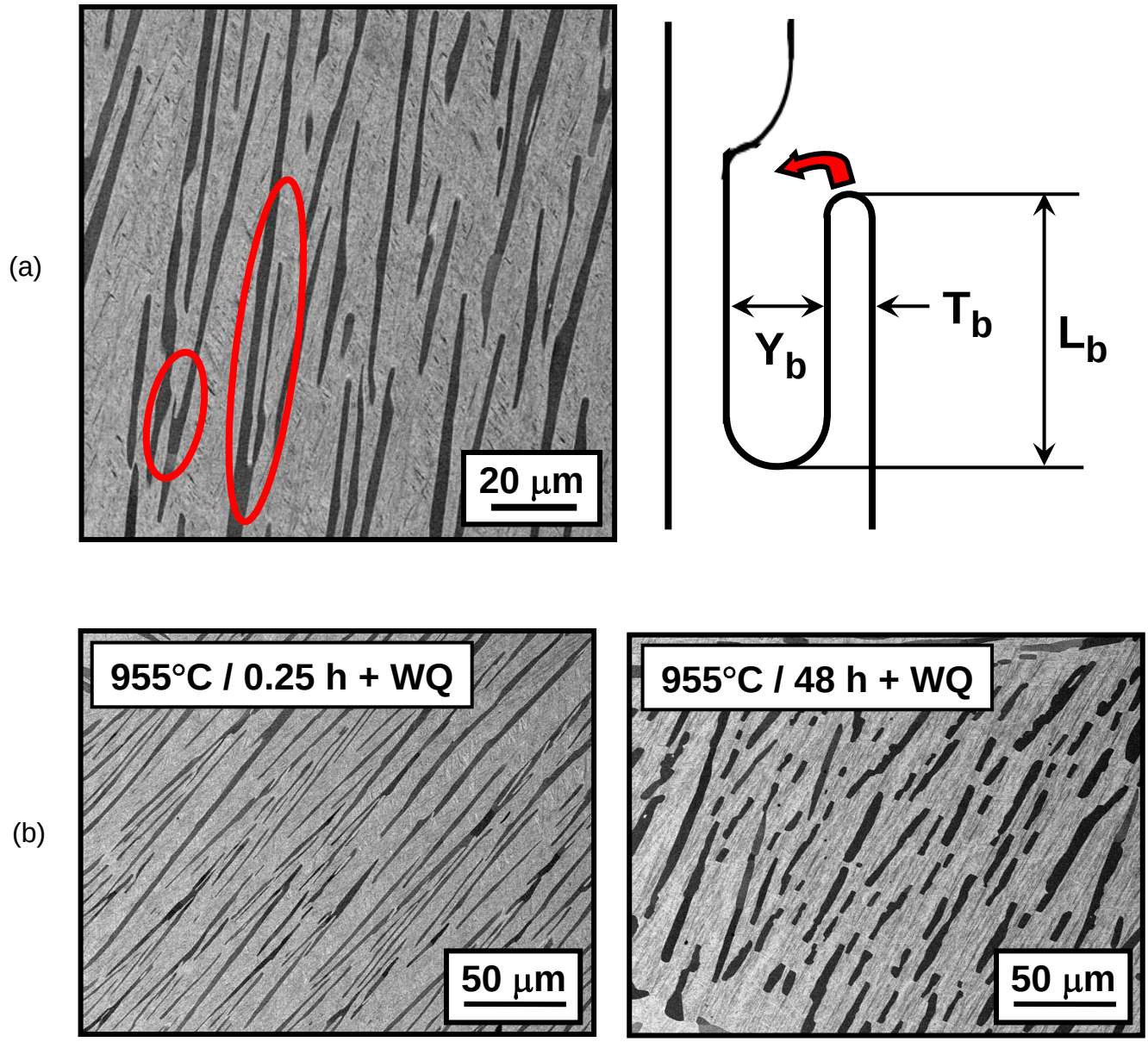

Figure 11. Static coarsening of a colony-alpha microstructure in Ti-6Al-4V: (a) SEM backscattered micrograph illustrating lamellar branching observed at 955°C and the idealized geometry used to describe the microstructure [49] and (b) SEM backscattered micrographs of samples heat treated at 955°C for times of 0.25 or 48 h followed by water quenching.

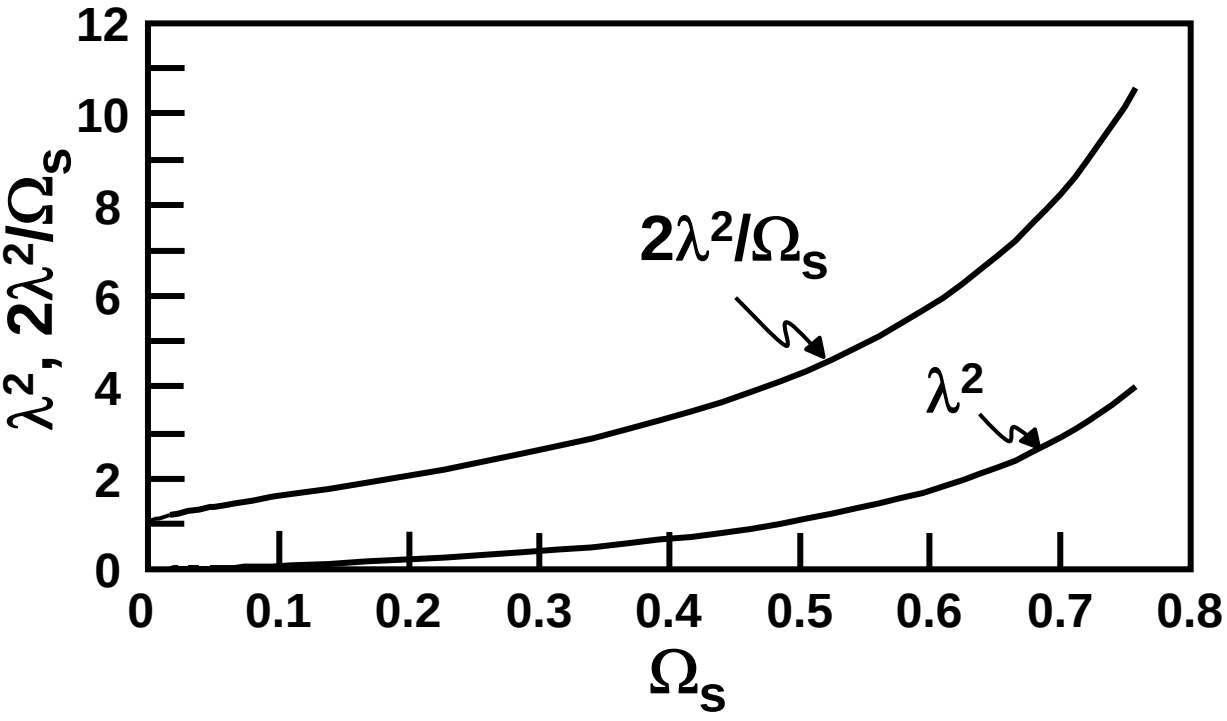

Figure 12. Dependence of the growth parameter λ^2 and the ratio $2\lambda^2/\Omega_s$ on the supersaturation Ω_s [52].

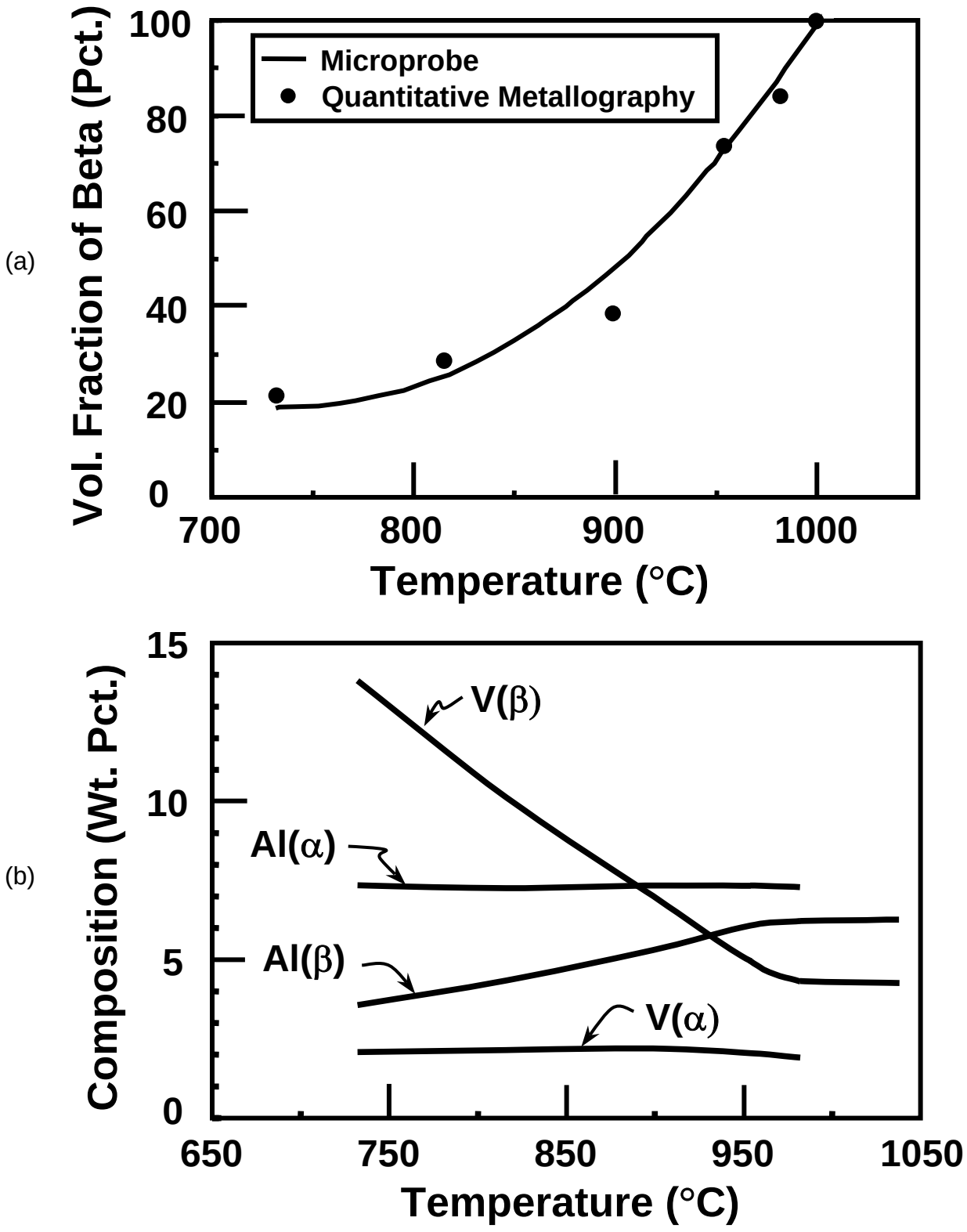

Figure 13. Phase equilibria data for Ti-6Al-4V with a regular interstitial level: (a) Beta-approach curve and (b) phase compositions [52].

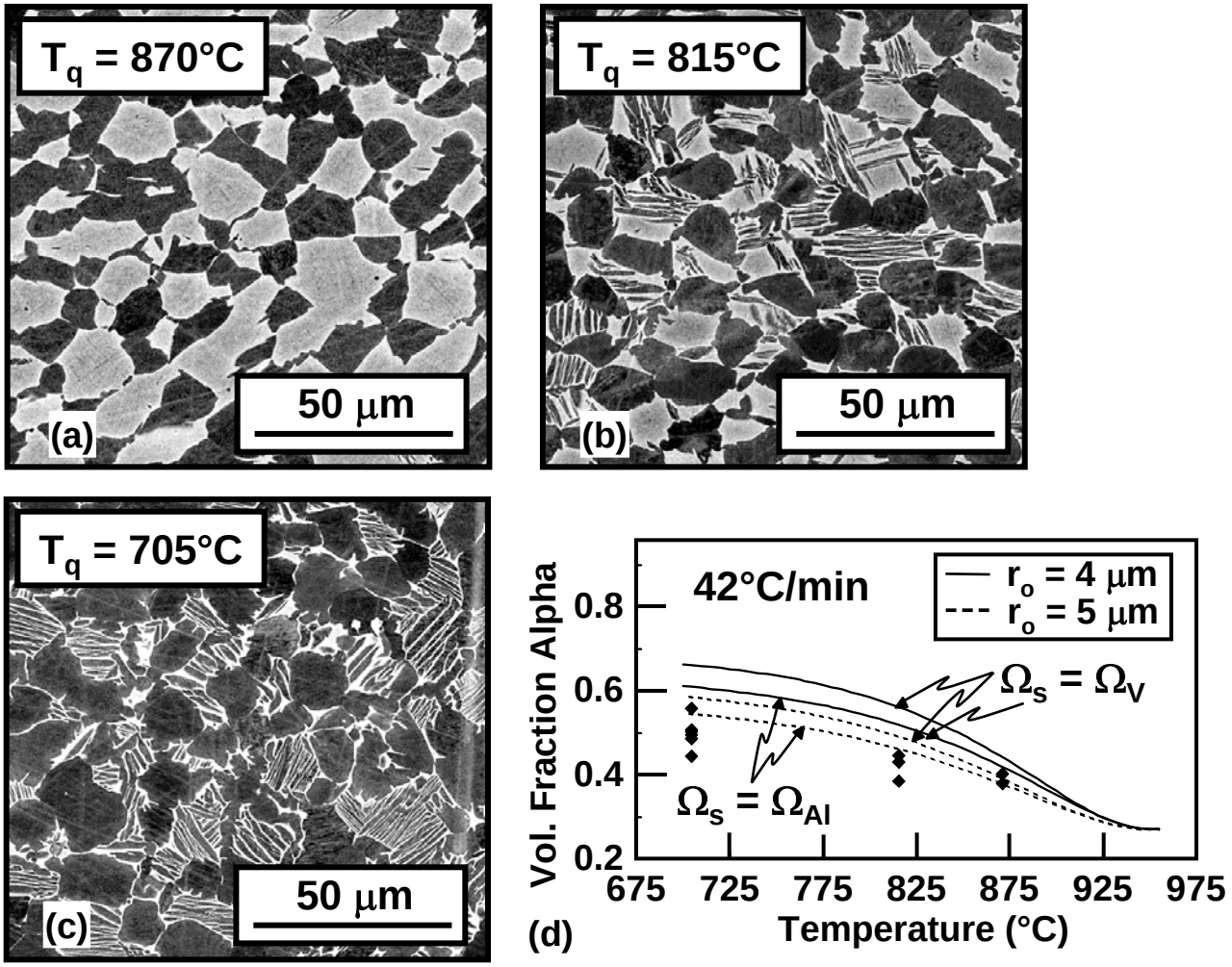

Figure 14. Alpha/beta heat treatment results for Ti-6Al-4V: (a,b,c) SEM backscattered micrographs of samples solution treated at 955°C, cooled at 42°C/min, and water quenched at the temperatures (T_q) indicated and (d) comparison of corresponding measurements of the volume fraction of primary alpha (data points) and diffusion-model predictions (lines) [52].

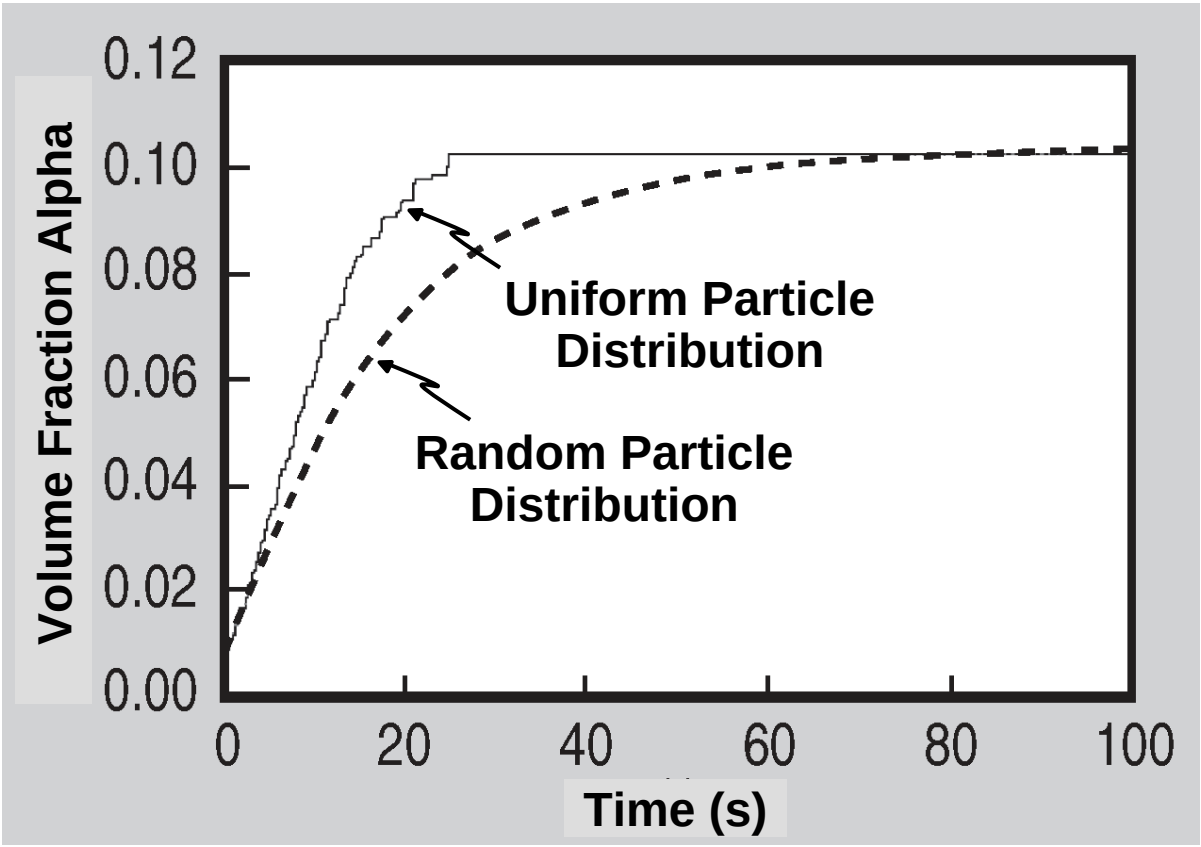

Figure 15. Phase-field model predictions of the growth of primary alpha in a titanium alloy which was solution treated at 930°C then cooled rapidly and soaked isothermally at 900°C. Simulations were done for an initial alpha-particle distribution that was random or uniform [59].

(a)

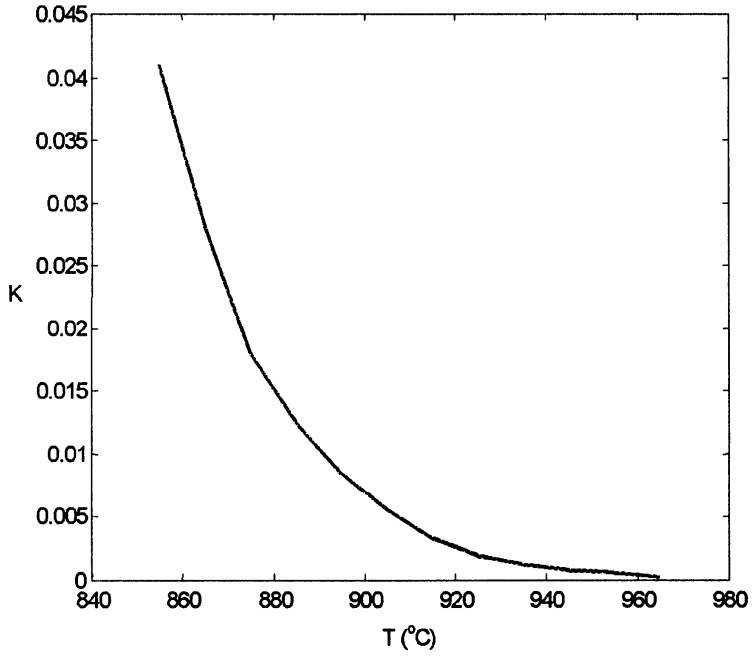

(b)

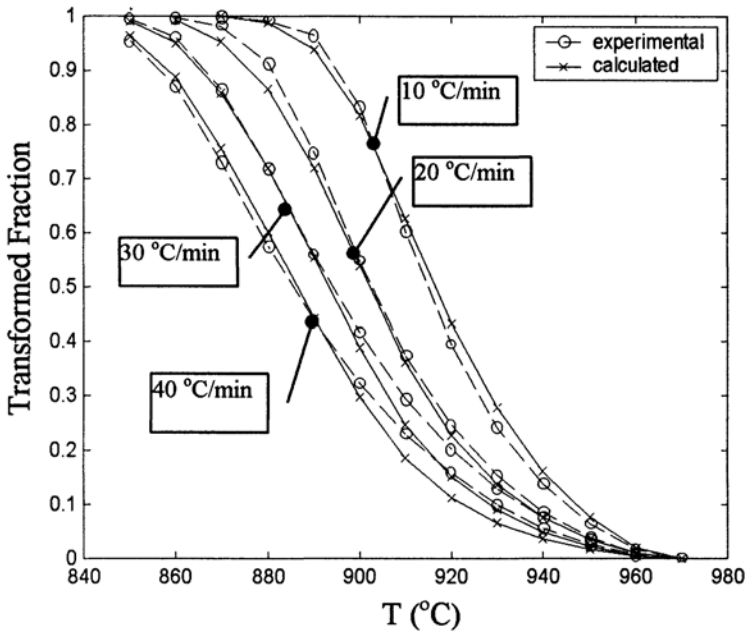

Figure 16. Application of the JMAK relation to predict cooling-transformation behavior of Ti-6Al-4V following beta annealing: (a) Fitted dependence of the rate constant k on temperature and (b) comparison of predicted and measured transformed fractions as a function of cooling rate and temperature [64].

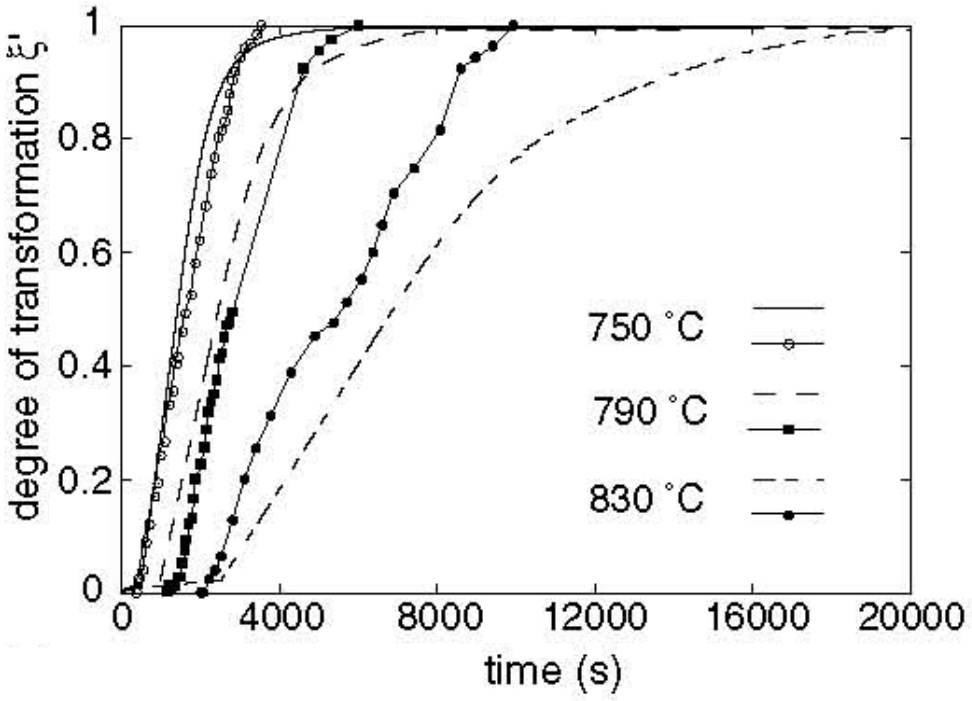

Figure 17. Comparison of measured (solid lines, data points) and predicted (broken lines) isothermal transformation kinetics for the titanium alloy Beta-Cez [68].

(a)

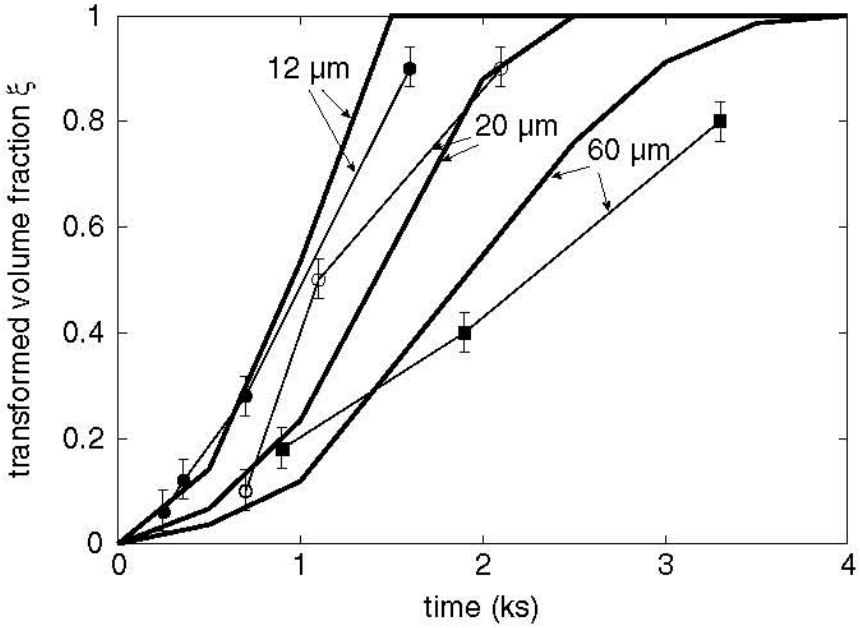

(b)

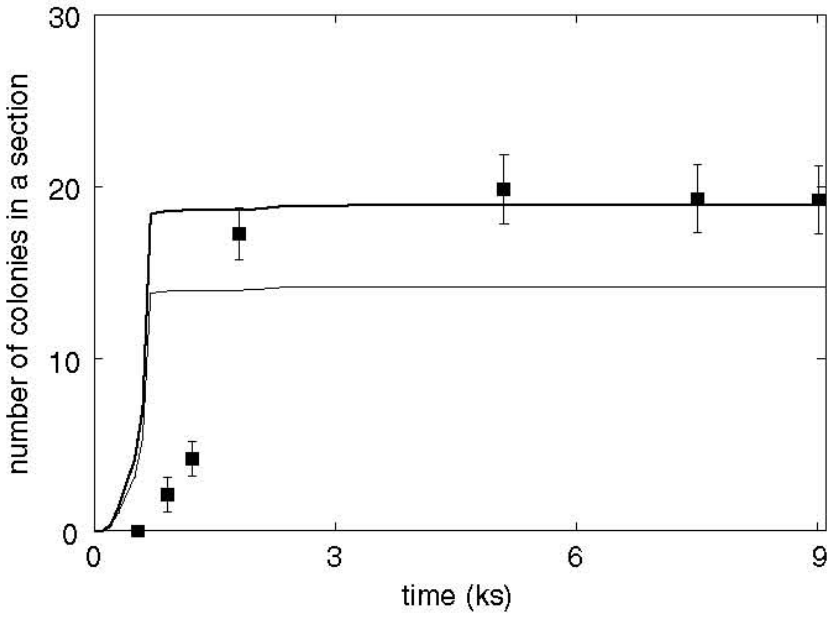

Figure 18. Comparison of measurements (data points, gray lines) and mesocale-model predictions (black lines) of microstructure evolution in Beta-Cez: (a) Isothermal transformation kinetics at 800°C for material prior beta worked to develop different subgrain sizes and (b) number of colonies observed in a 2D section as a function of time at 790°C for material pre-deformed 25 pct. in the beta phase field at a strain rate of 0.01 s^{-1} [69].